2013

Monitoring Wear In Sliding Surfaces By Using Acoustic Emission Signals

A.B.M. Iftekharul Islam
North Carolina Agricultural and Technical State University

Monitoring Wear in Sliding Surfaces by Using Acoustic Emission Signals

A.B.M. Iftekharul Islam

North Carolina A&T State University

A thesis submitted to the graduate faculty

in partial fulfillment of the requirements for the degree of

MASTER OF SCIENCE

Department: Mechanical Engineering

Major: Mechanical Engineering

Major Professor: Dr. Mannur J. Sundaresan

Greensboro, North Carolina

2013

The Graduate School
North Carolina Agricultural and Technical State University
This is to certify that the Master's Thesis of

A.B.M. Iftekharul Islam

has met the thesis requirements of
North Carolina Agricultural and Technical State University

Greensboro, North Carolina
2013

Approved by:

Dr. Mannur J. Sundaresan Major Professor	Dr. Devdas M. Pai Committee Member
Samuel P. Owusu-Ofori Department Chair	Dr. Albert Esterline Committee Member

Dr. Sanjiv Sarin
Dean, the Graduate School

Biographical Sketch

A.B.M. Iftekharul Islam was born at Natore, Bangladesh in 21st December, 1984. He completed his bachelor's degree in mechanical engineering from Bangladesh University of Engineering & Technology, Dhaka, Bangladesh in 2007. His undergraduate research was concentrated on experimental investigation of a structural material. Currently he is a candidate for Master of Science degree in Mechanical Engineering from North Carolina A&T State University, Greensboro, North Carolina, USA. He conducted his Masters research on Structural Health Monitoring focused on acoustic emission signal analysis for different affecting parameters on friction.

Dedication

I dedicate my current research work to my parents, who always inspired me to go for achieving higher academic excellences.

Acknowledgements

The ownership of all praises goes to Almighty Allah. I believe what I achieve in my life is His mercy. I would like to express my deepest gratitude to Dr. Mannur J. Sundaresan, who is not only my graduate advisor but also a continuous source of inspiration to thrive for research excellence. His guidance, support and advice are the key to continue my masters study as well as to carry out my research. I am also thankful to my thesis committee members: Dr. Devdas M. Pai & Dr. Albert Esterline for their valuable time and constructive critiques without which this thesis would be incomplete. I would also like to thank my colleagues at the Intelligent Structures and Mechanisms (ISM) lab for their cordial cooperation throughout my master's study.

Table of Contents

List of Figures ix

List of Tables xii

List of Abbreviations xiii

Abstract 2

CHAPTER 1 Introduction 3

1.1 Objectives 3

1.2 Motivation of the work 3

1.3 Structural Health Monitoring for Machine Parts 4

1.4 AE Technique for SHM 5

CHAPTER 2 Literature Review 7

2.1 Wave Propagation in Plate 7

2.2 AE Signal 9

2.3 Basis of AE Waveforms Analysis 10

2.4 Surface Roughness Parameters 12

2.5 Wear of Surface 13

2.6 Previous Study of Friction Related AE 14

CHAPTER 3 Experimental Methodology 17

3.1 Introduction 17

3.2 Test Materials 17

3.2.1 Main Bar. 17

3.2.2 Friction Pad. 18

3.3 Test Equipments 19

3.3.1 Sensors. 19

3.3.2 Preamplifier. 19
3.3.3 Load Cell. 20
3.3.4 MTS Machine. 21
3.3.5 Oscilloscope. 21
3.3.6 Fixture 21
3.4 Experimental Procedure 22
3.4.1 Sensor Bonding. 22
3.4.2 Lead Break Test. 22
3.4.3 Test Control Parameters. 22
3.5 Data Processing 24
3.5.1 Data Acquisition Setup. 24
3.5.2 Data Analysis 25
3.5.3 Source Location Determination 25
3.6 Damaged Surface Analysis 27
3.6.1 Measurement of Roughness Change. 27
3.6.2 Data Analysis 27
CHAPTER 4 Results & Analysis 28
4.1 Introduction 28
4.2 Comparison of AE at Different velocities 28
4.3 Comparison of AE at Different Roughness 32
4.4 Comparison of AE at Different Normal Pressures 34
4.5 Variation of Waveform 37
4.5.1 Variation of Waveform within a Test 37
4.5.2 Variation of Waveform with Changing Velocity 39
4.5.3 Variation of Waveform with Changing Roughness 40

4.5.4 Variation of Waveform with Changing Normal Pressure 43
4.6 Observation of Change in Surfaces Topography 45
4.7 Variation of Roughness Changes 48
4.8 Calculation of Damaged Area 50
4.9 Analysis of Results 51
CHAPTER 5 Discussion and Future Research 55
References 57
Appendix A 60
Appendix B 61

List of Figures

Figure 2.1 A schematic illustrating the motion pattern of Lamb waves in a solid plate of thickness 2d..... 7

Figure 2.2 Dispersion curves for a traction free aluminum plate. 8

Figure 2.3 This AE source & detection.. 9

Figure 2.4. AE features extracted from each hit 11

Figure 3.1. Main bar with central frictional area. 17

Figure 3.2. Friction pad..... 18

Figure 3.3 Bonded PZT sensor with electrode..... 18

Figure 3.4 Preamplifier. 20

Figure 3.5 Load cell. 20

Figure 3.6 MTS machine 21

Figure 3.7 Schematic representation of the test fixture 22

Figure 3.8 Test amplitude and frequency 23

Figure 3.9 PCI-2 data acquisition setup 24

Figure 3.10 Experiment flow chart 25

Figure 3.11 Source location technique 26

Figure 3.12 Surface Profiler..... 27

Figure 3.13 Optical microscope. 27

Figure 4.1 Amplitude distribution of different velocity AE events 30

Figure 4.2 Cumulative events & AE energy at different velocities 31

Figure 4.3 Comparison of surface roughness on AE at low velocity (at 2 MPa pressure). 32

Figure 4.4 Comparison of surface roughness on AE at high velocity (at 2 MPa pressure). 32

Figure 4.5 Comparison of surface roughness on AE at low velocity (at 4mpa pressure)..... 33

Figure 4.6 Comparison of surface roughness on AE at high velocity (at 4mpa pressure). 33

Figure 4.7 Comparison of normal load on AE at low velocity (for smooth surface pairs) 34

Figure 4.8 Comparison of normal load on AE at high velocity (for smooth surface pairs) 35

Figure 4.9 Comparison of normal load on AE at high velocity (for smooth surface pairs). 36

Figure 4.10 Comparison of normal load on AE at high velocity (for smooth surface pairs). 36

Figure 4.11 Variation of waveform of high velocity rough pair 2 MPa test during 100 cycles... 37

Figure 4.12 Variation of waveform of high velocity rough pair 2 MPa test during 300 cycles... 37

Figure 4.13 Variation of waveform of high velocity rough pair 2 MPa test during 1000 cycles. 38

Figure 4.14 Variation of waveform of high velocity rough pair 2 MPa test during 3000 cycles. 38

Figure 4.15 Waveform of low velocity smooth pair 2 MPa test..... 39

Figure 4.16 Waveform of medium velocity smooth pair 2 MPa test..... 40

Figure 4.17 Waveform of high velocity smooth pair 2 MPa test..... 40

Figure 4.18 Waveform of medium velocity smooth pair 2 MPa test 41

Figure 4.19 Waveform of medium velocity rough pair 2 MPa test. 41

Figure 4.20 Waveform of low velocity smooth pair 4MPa test..... 42

Figure 4.21 Waveform of low velocity rough pair 4MPa test 42

Figure 4.22 Waveform of low velocity rough pair 2 MPa 43

Figure 4.23 Waveform of low velocity rough pair 4MPa test 43

Figure 4.24 Waveform of high velocity smooth pair 2 MPa test..... 44

Figure 4.25 Waveform of high velocity smooth pair 4MPa test..... 44

Figure 4.26 Undamaged smooth surface. 45

Figure 4.27 Effect on smooth surface-2 MPa normal pressure after 3000 Cycle. 45

Figure 4.28 Effect on smooth surface-4MPa normal pressure after 3000 Cycle. 46

Figure 4.29 Undamaged rough surface. 47

Figure 4.30 Effects on rough surface-2 MPa normal pressure after 3000 Cycle. 47

Figure 4.31 Effect on rough surface-4MPa normal pressure after 3000 Cycle. 48

Figure 4.32 Change of roughness by friction for rough-rough pairs 49

Figure 4.33 Change of roughness by friction for smooth-smooth pairs. 49

Figure 4.34 Calculation of damaged area. 50

List of Tables

Table 2.1 Signal Parameter Effect 11

Table 2.2 Wear Type Identification 13

Table 3.1 Friction Test Combinations 23

Table 3.2 Signal Acquiring Parameters 24

Table 3.3 Source Location Chart 26

Table 4.1 Maximum Axial Load in Newton for different tests 28

Table 4.2 Chart for Calculating Deterministic Pressures for Different Tests 50

List of Abbreviations

SHM	Structural Health Monitoring
AE	Acoustic Emission
FE	Finite Element
PZT	Piezoelectric material
MTS	Material Test System
NDE	Nondestructive Evaluation
S_0, S_1, S_2	Symmetric Modes
A_0, A_1, A_2	Anti-symmetric Modes
ISM	Intelligent Structure & Mechanisms
S2	Smooth pair 2 MPa test
S4	Smooth pair 4 MPa test
R2	Rough Pair 2 MPa test
R4	Rough Pair 4 MPa test
R_a	Average roughness
R_q	Root Mean Square Roughness
R_t	Maximum Peak To Valley Height
R_z	Height Parameter
TTS	Tribologically Transformed Structure
Msps	Mega sample per seconds

Abstract

Machine parts that are in relative motion often face a state of friction in their applications. The friction, when it is uncontrolled, can cause the machine part surfaces to degrade severely. At the time of service of a machine, relative motion between surfaces sometimes can cause crack growth of fretting fatigue. Conventional methods for determining the degree of deterioration and potential crack growth formation in in-situ application have not been proven sufficiently effective. Acoustic emission (AE) based Structural Health Monitoring (SHM) has the potential for real-time detection of damage growth in structures. But in the case of sliding contact between two surfaces, the relative motion encounters extraneous noise. In this research, two parallel bonded PZT sensors were used for detecting AE signals from sliding contacts. The time interval technique was taken into consideration to determine the authenticity of the hit source location, which reduced the noise data. Different parameters such as sliding velocities, normal pressure, and surface roughness were considered to determine their corresponding effect on AE signals. The nature of the waveforms in terms of frequency components present in the signal is also discussed. In this study, a surface profilometer was used to measure the change of roughness due to friction. Optical microscope images were taken to understand wear mechanisms involved in the wear of the friction surfaces. The dependence of the parameters on AE signals found in this research can be an effective tool for monitoring the early stages of wear in sliding contact.

CHAPTER 1

Introduction

1.1 Objectives

The primary objective of this study is to monitor the health of machine parts that are in sliding contact with the help of AE signals. For this reason, it is necessary to characterize the AE signal with changing parameters. The objectives in this study are summarized as follows:

1. To determine the effect of changing sliding velocity on AE signals
2. To identify the change of AE signals with different normal pressures
3. To understand the nature of AE data if the surface roughness values are varied
4. To obtain a relationship for each of the above three parameters in terms of the nature of the waveforms
5. To correlate the damage with changed roughness values

1.2 Motivation of this Work

The Structural Health Monitoring (SHM) of the machine parts which are in relative motion has created a real challenge for researchers. Application of SHM to sliding surfaces is not as easy as applying SHM to static structures. The monitoring techniques for these sliding parts are still in the incipient stage now. Many systems use the large transfer particles produced from a significant damage of the structures for condition monitoring. Magnetic chip detection and some similar techniques carry the information of bearing chambers of aircraft engines when these bearings are damaged due to friction. These conventional techniques are good for saving the total system by reporting after some damage is done to a critical extent in a part. However, these techniques cannot give information when friction is occurring at primary levels. They also do not give enough forecast before the part is being damaged.

If one's eyes are closed, the voice of one's friend is easily recognized. The current research was inspired with this daily event. This very basic feature of listening skill utilizes the frequency components of every human being which is identical for each person. Basically, science is using the pattern of acoustic signals to identify the person. Signal pattern can also easily be interpreted into useful information for other events. Every single mechanical movement creates a pressure wave of its kind. In a certain span of frequency range it is audible to human ear. For collisions in micro level, that are very usual of the machine parts with relative motions, cannot be reached by human ear. But with the help of AE sensors we can collect those signals. The long lasting problem for monitoring health of sliding contacts and a potential way to solve the problem is the main source of inspiration for this study.

1.3 Structural Health Monitoring of Machine Parts

SHM is one of the most focused branches of modern technology. Conventional nondestructive evaluation (NDE) faces difficulties to provide information for the structure while it is running or in service. In these cases, SHM is being used as an effective tool to not only understand the current condition, but also to predict imminent failures. Nowadays, SHM is a very common technique for monitoring large structures such as bridges, aircraft wings, etc. However, it is very challenging to apply SHM to small mechanical parts that are in relative motion such as bearings, engine pistons, gas turbine blades, etc.

The present industrial practice for checking the conditions of machine parts with relative motion is to inspect them periodically with NDE tests to find faults, though this technique is only applicable when the machines are stationary. Stopping the machine is not always desirable for several reasons. The first reason is that, we cannot simulate the real functional situations faced by structural parts in relative motion while testing. Moreover, the time taken for NDE testing is

also a factor. The moving parts must be out of operation for the inspection which is often very costly in a continuous production plant.

Among the different types of NDE tests such as eddy current or radiography, the acoustic emission (AE) generated by structures is the most effective way to get current information. The reason is that we can easily convert sound waves into electrical voltage by piezoelectric materials. The main problem for the case of monitoring structures with running conditions is the inability to isolate the desired data from other signals. There occur multiple events at a time, from which the detrimental effect is difficult to detect.

1.4 AE Technique for SHM

AE is a phenomenon of sound and ultrasound waves released from the stress in materials that have undergone elastic collisions, plastic deformation or fracture processes. The concept of taking sound as a tool of understanding the condition of a structure is an ancient one. A material may be struck to hear a sound to test whether it is metal or not, potters check their art crafts quality by creating a sound, and even modern age doctors slap patients' bellies to perceive the inside conditions. However, the use of ultrasound, which cannot be heard by humans, is a relatively new technique to examine the structural integrity. It evolved with creating and detecting devices (Piezoelectric materials) of ultrasound by Currie brothers in 1880.

> "The Currie brothers were able to generate mechanical stress in response to an applied voltage on a quartz crystal. These crystals allowed for the generation, and subsequent reception, of pressure waves in the Mega Hertz frequency range and without such a crystal generation of pressure waves in the ultrasound frequency range would be impossible. "

https://wiki.engr.illinois.edu/display/BIOE414/The+History+of+Diagnostic+Ultrasound

Since the Currie brothers efforts, ultrasound has been used as a reliable diagnostic tool for nondestructive evaluations. Though AE is being used to find faults in static structures, it is not perfectly utilized for in-situ application. It is crucial to filter out the surrounding noise. If a high threshold value is applied to sensing devices for avoiding the noise signals, the signals of interest may eventually be missed.

CHAPTER 2

Literature Review

2.1 Wave Propagation in Plates

A wave is generated by the oscillation or disturbance in a medium through which energy is transferred. The usual types of wave are longitudinal and shear, or transverse, wave. For longitudinal waves, the displacement of the medium particle is parallel to the direction of the propagation of the wave. In the case of the shear wave, the particle motion of the medium is perpendicular to the direction of wave propagation.

The fundamental difference between bulk medium and plate waves is that plate waves are constrained by boundaries. For a finite plate length, the plate wave is termed as a guided wave. In the case of the guided wave, there occur interactions with boundaries by reflection, refraction, and mode conversion between longitudinal and shear waves. The partial differential equations for the guided wave are the same as for the bulk wave, but the boundary conditions lead to solutions of different forms which are named by their inventors such as Lamb, Raleigh, or Stonely (Rose 2004).

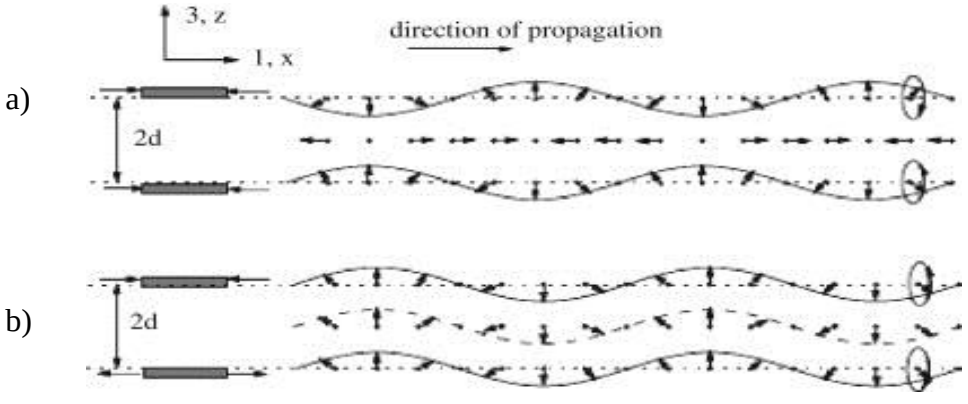

Figure 2.1. A schematic illustrating the motion pattern of Lamb waves in a solid plate of thickness 2d:

(a) Symmetric mode and (b) anti-symmetric mode, (Diamanti and Soutis 2010).

For the wave propagation in a finite thickness material Lamb wave equations are dominating. The particle movement for the medium is elliptical for Lamb wave. There are two modes for Lamb wave propagation in plates for isotropic materials. Modes are created due to different directions of particle displacement through the thickness. A plane strain condition is considered in the case of Lamb waves. The traction forces on both the top and bottom surfaces are considered to be equal to zero. The boundary conditions lead to two equations, one each for the symmetric and anti-symmetric modes (Figure 2.1).

The velocity of Lamb waves inside the plate is not constant. The velocity depends on the frequency and the elastic property of the plate material. In practice, the parameter used in this regard is the product of plate thickness and frequency. Each thickness-frequency product results in different velocity values. These velocity dispersions are varied in terms of order. For higher frequencies, higher modes are seen. However, the zero-order modes are common for any frequency.

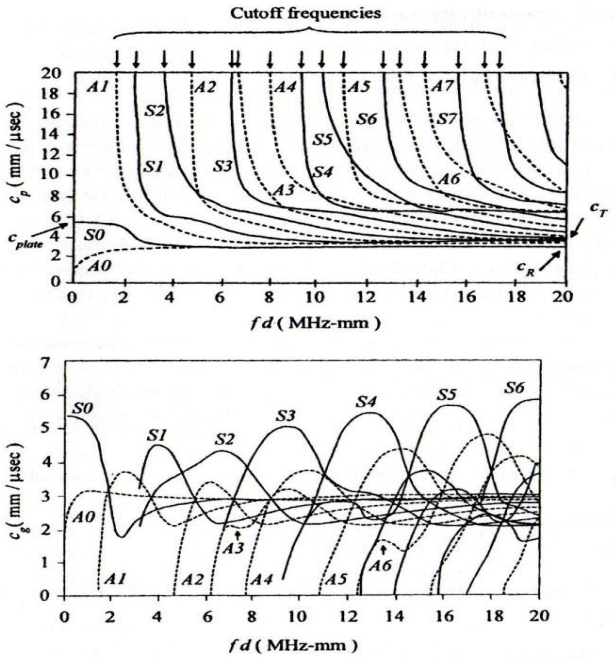

Figure 2.2. Dispersion curves for a traction free aluminum plate (Rose 2004)

When a longitudinal wave hits an interface (such as a plate boundary) at an angle, particle movement in the transverse direction may occur. When the wave is reflected in a boundary surface It leads the longitudinal wave transforming into shear and another, longitudinal wave. This phenomenon is termed as mode conversion and is very common in the case of wave propagation through a plate.

2.2 AE Signal

The release of stress in AE is transferred through the material in the form of elastic waves or heat. The elastic wave, when it goes beyond a certain frequency (1 kHz), is known as an AEsignal. AE is detected by a transducer, which is generally operated by electromechanical principles (Figure 2.3).

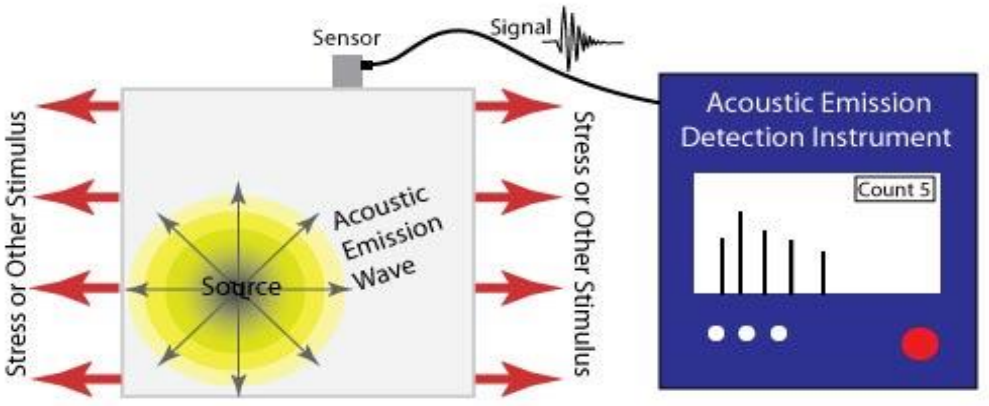

Figure 2.3. AE source & detection http://www.ndt-ed.org/EducationResources/CommunityCollege/Other%20Methods/AE/AE_Theory-Sources.htm

Depending upon the amplitude distribution of signals, there are mainly two types of AEs: continuous and burst. The continuous signal occurs steadily in a typically low level, repetitive manner (Vahaviolos 1999). High signal density emission is observed in a repetitive case. Noise is an example of a continuous signal. Arthur E. Lord, Jr. suggested that continuous emissions arise from dislocations moving through the crystal and possibly slip movements (Mason 2012).

The burst type emission is a discrete signal that is considered to be a single event. According to Arthur E. Lord, Jr., AEs are associated with twinning, micro-cracks, and larger plastic strains. In the case of friction, which is actually a collision or breakage of asperities on the micro level, burst type emissions carry more information about the change of the surface.

2.3 Basis of AE Waveform Analysis

To acquire AE signals in a meaningful way, it is necessary to define a set of selection criteria so that the burst signal can be easily distinguished from noise and other continuous signals. The first important point is to select specific amplitudes as threshold values. The threshold may be fixed or floating, depending upon the nature of the noise level. After distinguishing a burst type signal, characterization is needed to extract features so that it can easily compared with other similar signals. Three basic features are extracted: amplitude, duration, and frequency. The purpose of feature extraction is to collect information about the shape and content of the waveform to differentiate it from other waveforms with different source mechanisms (Miller et al. 2005). Moreover, as AE is the rapid release of energy in a material, the energy content of the AE signal is related with the amount of energy released. In this way, the energy calculation is a good means of characterizing the AE.

There are mainly three parameters to determine AE hits: hit definition time (HDT), hit lockout time (HLT), and peak definition time (PDT). HDT is the maximum time between threshold crossings. HLT is the time that is passed after a hit has been detected and before a new hit can be detected. PDT is the time allowed, after a hit has been detected, to determine the peak value (Figure 2.4).

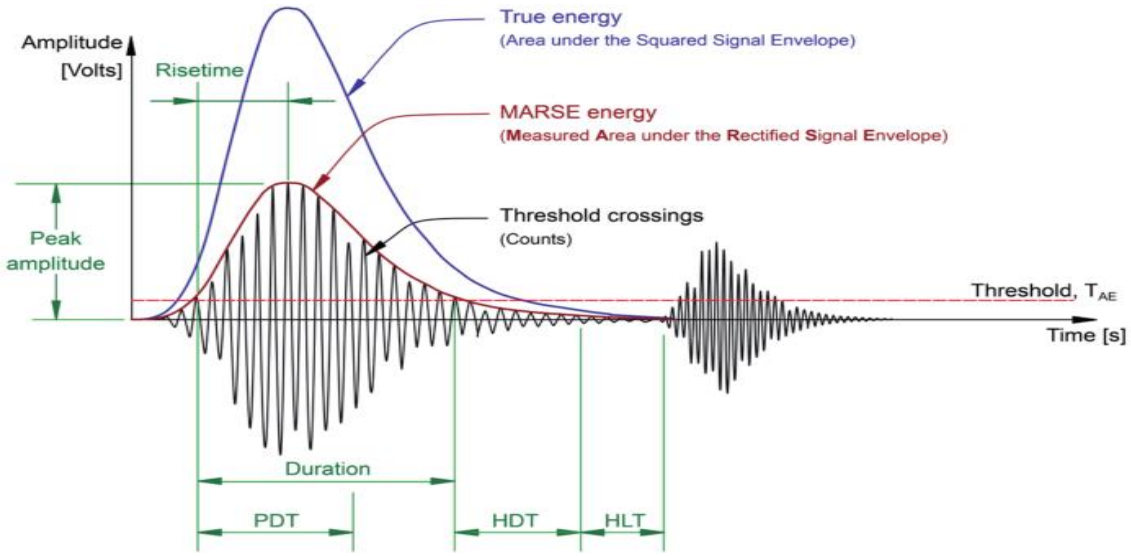

Figure 2.4. AE features extracted from each hit (Unnþórsson, 2013).

According to R. Unnþórsson (2013), the effects of signal parameter setup criteria can be outlined by Table 2.1. The optimum conditions for setting up these parameters depend on systems from where the AE events are coming. The features described in Table 2.1 and Figure 2.4 are from hit driven methodology. To extract the change of AE features trend with respect to time, a time driven method is to be considered.

Table 2.1

Signal Parameter Effect

Condition	**Effect**
HDT too High	Two hits may be considered as one
HDT too low	System may not fully capture AE hit
PDT too low	True peak may not be identified
PDT too High	False measurement of peak value may occur
HLT too low	System may capture reflections and late arriving components as a hit
HLT too High	The system may not capture next AE

2.4 Surface Roughness Parameters

Roughness is one of the important tools used to characterize surface conditions. Roughness can be controlled by grinding the surface. Roughness is a measure of deviation of ideal surface in the vertical direction. There are many terms that are used in literature to describe roughness profile of a surface. The following are some important parameters to define roughness:

Average roughness, R_a: the arithmetic mean of the deviation of the profile normal to the surface from the mean line. By definition, the R_a value should be zero. Mathematically, for a surface of length *l*,

$$R_a=\frac{1}{l}\int_0^l |z(x)|dx \tag{2.1}$$

Here, z is the distance measured in normal direction of a surface

Root Mean Square Roughness, R_q: the standard deviation of the distribution of surface heights. R_q is an important parameter to describe the surface roughness by statistical methods (Gadelmawla, 2012).

$$R_q=\sqrt{\frac{1}{l}\int_0^l \{z(x)\}^2 dx} \tag{2.2}$$

Maximum Peak To Valley Height, R_t: the height difference between maximum peak to minimum valley in a sample length (Whitehouse 2004)). The value of R_t may be varied for considering different sample length.

Height Parameter, R_z: the average of five height differences between highest peaks and lowest valleys within a sample length. The number of points that are considered here is ten. R_z is actually the average of R_t.

$$R_z=\frac{1}{5}\left(\sum_{i=1}^{i=5} z_{peak} - \sum_{i=1}^{i=5} z_{valley}\right) \tag{2.3}$$

2.5 Wear of Surfaces

Wear is the removal of particles from the surface mainly caused by mechanical action. There are three main types of wear for sliding surfaces:

Adhesive wear: This wear is due to localized bonding between contacting solid surfaces leading to material transfer between the two surfaces or loss from either surface (ASTM G40-13). It is the most common form of wear for smooth bodies. The volume of adhesive wear is dominated by Archard's theory (Archard and Hirst 1956).

Abrasive wear: This wear is due to hard particles or hard protuberances forced against, and moving along, a solid surface (ASTM G40-13). When a rough hard surface or a soft surface containing hard particles slides on a softer material and plowing is created, the removal of material is termed as abrasive wear.

Table 2.2

Wear Type Identification

Wear Type	Unaided Eye	Microscopically
Adhesive wear	Rough, torn, melted or plastically deformed metal, bands or streaks	Rough, irregular surface
	High temperature oxidation	Metal from other surface adhering to other surface by spot tests or microprobe analysis
Abrasive wear	Scratches or parallel furrows in the direction of motion	Clean furrows, burrs, chips
	High rates of wear	Embedded abrasive particles

http://www.stle.org/resources/lubelearn/wear/

Corrosive wear: If material surface is corroded, the oxide layers become softer and mechanical action may easily remove them, leading to corrosive wear.

2.6 Previous Study of Friction Related AE

The AE generated from friction was studied by several researchers. (Baranov, Kudryavtsev et al. 1997) developed a theoretical model and used to correlate the affecting parameters with AE for sliding friction of solids. He also compared his model with the amplitude distributions of AE. The study can be regarded as a fundamental effort to describe the AE signal in tribological applications.

A theoretical scheme for signal processing and pattern recognition for AE from bearing friction was proposed by James Li and Li (1995). The implementation of this type of scheme faces many types of practical issues. For example, there were no significant means to avoid noise. The signal coming from the bearings presented in this paper is more or less a continuous signal. It is very difficult to identify a single hit and to differentiate the single hit from a noise signal.

Starting from the procedural issues to data acquisition issues, detecting AE signals from moving machine parts is a difficult task to perform. (Mba and Sikorska 2008) enlisted the challenges to apply AE technique for machine parts that are in relative motion. Most of the difficulties can be overcome with modern data acquisition techniques.

The effect of surface roughness and grinding angles on friction were compared with changed surface topography by Menezes, Kishore et al. (2008). They suggested the amplitude of stick-slip motion is higher for lubricated conditions. They described some features of friction damage mechanisms in relation to different grinding angles.

The relationship of fretting debris and AE dissipation energy was studied by Ito, Shima et al. (2009). They used a ball and a flat plate as specimens along with the TTS method to analyze results.

The relation between average coefficient of friction with change of grinding angle was outlined by Menezes, Kishore et al. (2006). Here it was suggested that the amount of material transferred is related with the grinding angles.

Modeling the AE from friction is relatively new. Elastic energy generated by asperity contact was modeled and validated by varying different contact loads by Fan, Gu et al.(2010). They suggested a model to estimate the contact load supported by asperities of the sliding contact using AE signals. The number of asperity contacts and the sliding velocity was compared with AE measured.

With a modified form of a pin-on-disk tribometer, Sun, Wood et al. (2005) used AE and the electrostatic approach to quantify wear amount. The experimental results showed a correlation between friction coefficient with AE root mean square (rms) value and electrostatic charge collected by sensors. They outlined three different wear zones seen on SEM and correlated them with average AE rms signal.

An experimental study with a defective bearing characterized the intrinsic periodicity aspect of AE signals for a rotating part, which is termed as cyclostationary, was carried out by Kilundu, Chiementin et al. (2011). If a machine part rotates, they assumed the AE from defects should somehow repeat in a cyclic order in some certain time interval. However, this assumption does not work for small defects. They suggested an AE frequency band from 100 kHz to 1 MHz.

The amount of wear and corresponding AE signal for different materials was studied by Hase, Wada et al. (2008). They also outlined the shapes of different wear particles. They suggested that transfer particles are the main source of AE for non-lubricated friction.

Hase, Mishina et al. (2009) showed correlation between the AE mean value the coefficient of friction. In another study, two types of wear mechanisms, adhesive and abrasive,

(Hase, Mishina et al. 2012) were represented to interpret AE signals features. They also outlined the AE frequency and voltage generated from different types of mechanical events such as sliding friction, abrasive wear, adhesive wear, and crack propagation.

In the case of sliding contact friction, the stick-slip phenomenon is very common. The AE features and their corresponding tribological behavior during stick-slip was studied by Ferrer, Salas et al. (2010). They found high amplitude signals during slip and also presented the nature of the frequency content.

To identify the rubbing frequency from other vibration and other noise signals, Benabdallah and Aguilar (2008) suggested a frequency band of 50 kHz to 2 MHz. They studied the friction coefficient and wear on dry and greased lubricated ball-on-cylinder systems. They used a varying parameter of sliding velocity.

Greenwood et al. (1966) modeled multi asperity theory to describe the elastic collisions of the surface peaks. A numerical simulation was carried out by Alam & Sundaresan (2010) [only one ref per sentence]. They characterized the waveform generated from the friction surface in terms of amplitude and frequency. The study reveals the frequency components, as well as symmetric and anti-symmetric parts of a friction signal. This study can be regarded as a theoretical basis of the current work.

Asamene & Sundaresan (2012) conducted a study on a friction bar with two pairing surfaces and two different normal loading conditions. The stick-slip phenomenon was found in the tests and more AE hits were found in the stick portion of rubbing. They performed this study on sinusoidal axial velocity. The effects of changing pressure and roughness on AE signals were also analyzed in this study.

CHAPTER 3

Experimental Methodology

3.1 Introduction

The friction tests were carried out on some preselected areas of the specimen bar and the shoe pad assembled on a fixture. The friction related AE was sensed by bonded PZT sensors. The setup was developed by the Intelligent Structures & Mechanisms (ISM) lab and it is different than the typical pin-on-disk tribometer friction tester. There was a setup for acquiring and storing AE data. The tests were conducted by keeping the bar stationary and the fixture and pad oscillating. Oscillatory motion and velocity of friction were created for this study.

3.2 Test materials

3.2.1 Main Bar. The bars were A2 Tool Steel in composition. Each bar had a middle area of controlled roughness and grinding direction. The center area of the bar was used to conduct friction tests. The two bonded PZT sensors were located 152.4 mm apart (Figure 3.1). Between these two sensors, friction tests were carried out. For each test, an undamaged surface was used. The Rockwell hardness value for the steel bar was HRB 96. The thickness of the bar used was 3 mm. The grinding direction of the bar was 0° in relation to the longitudinal axis of the bar.

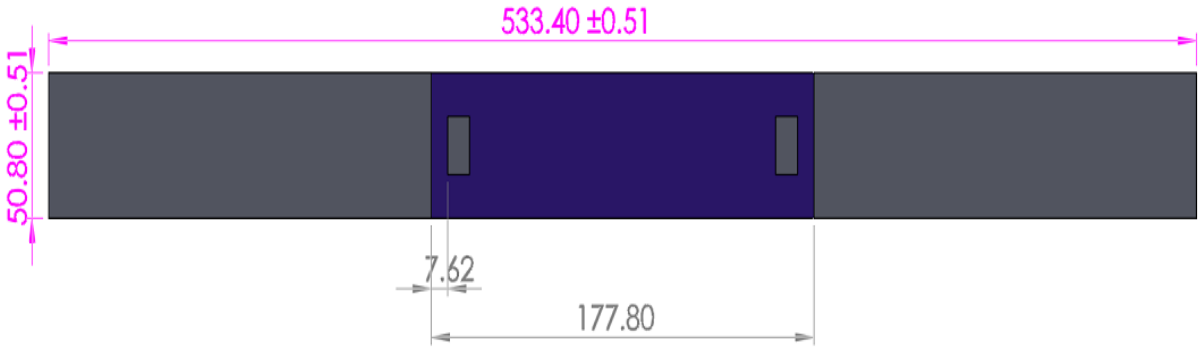

Figure 3.1. Main bar with central friction test area

3.2.2 Friction Pad. The pads were made of A2 Tool Steel. They were machined to obtain a certain friction area with the same roughness as its corresponding bar. This allowed us to achieve the condition where surfaces with the same roughness were rubbing against each other. The grinding direction of the pad was 0° in relation to its own longitudinal axis. The Rockwell hardness value for the pads was HRB 123.

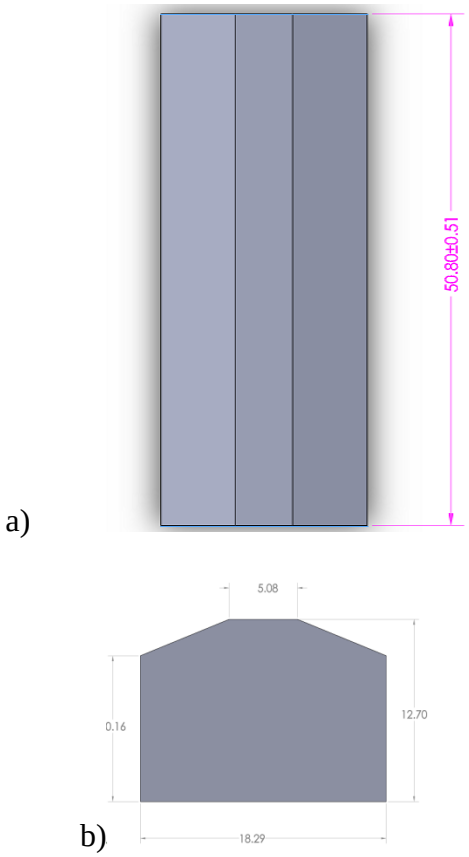

Figure 3.2. Friction pad a) top view, b) side view

Figure 3.2 describes the two views of the friction pads that are used in this study. All dimensions described in the figures are in millimeters. The contact surface of the pad for friction was made narrower than previous study Asamene and Sundaresan (2012). This design was developed to decrease the amount of load needed to create same pressure. This design allowed minimizing the buckling of the bar during normal loading.

3.3 Test Equipment

3.3.1 Sensors. The sensor for collecting AE signal used here was a bonded PZT type. It was fabricated in the lab. The material used was a PSI-5A4E Piezo-ceramic. It had a main body of PZT material and an electrode. It is described in Figure 3.3 where all dimensions are in millimeters. The PZT body was etched on the top of the surface except beneath the electrode. The electrode used for this PZT sensor was a steel foil with 3 mm width and 0.0254 mm thickness. The sensors were bonded to the main friction bar to collect AE signals. The working range of the sensor was 100 to 700 kHz.

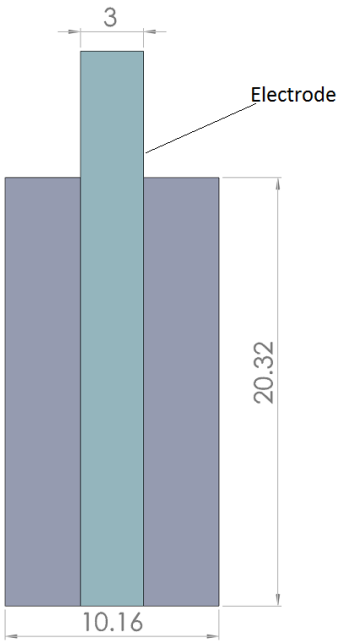

Figure 3.3. Bonded PZT sensor with electrode

3.3.2 Preamplifiers. The energy harvested by the sensors was very low. In this study, Physical Acoustic Corporation's 2/4/6 preamplifiers were used to amplify this low signal (Figure 3.4). Options to multiply signals were for 20 dB, 40 dB and 60 dB which are 10X, 20X and 1000X amplification respectively. The band-pass filter within the preamplifiers was 100-400 kHz and the high-pass filter was 50 kHz.

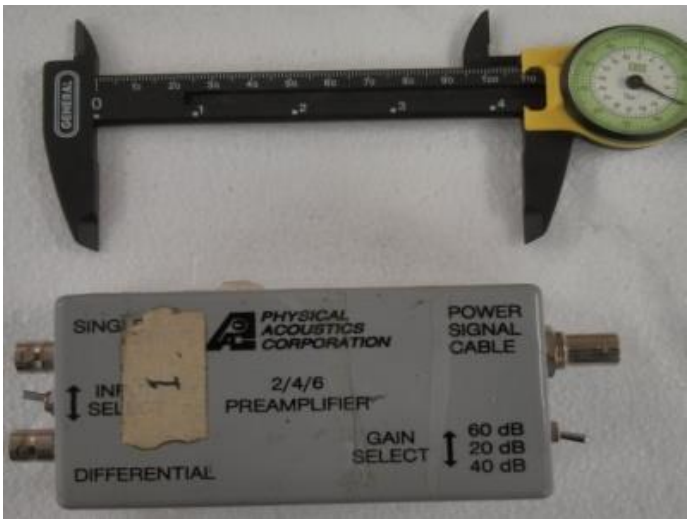

Figure 3.4. Preamplifier.

3.3.3 Load Cell. A load cell with a capacity up to 500 kg was used to adjust the pressure on the contact surface (Figure 3.5). The load cell is actually a transducer that converts mechanical force into electrical potential by the use of a strain gauge. The voltage is generated by the deformation of strain gauge. The change of pressure creates a change in electrical resistance of the wire of the strain gauge. A calculation which is shown in Appendix A was to determine the equivalent voltage which is produced by a specific applied pressure.

Figure 3.5. Load cell

3.3.4 MTS Machine. The 810 Model universal testing machine from the Material Testing Service Company was used (Figure 3.6). The MTS had a maximum load limit of 89 Kilo Newton. The machine was controlled through the use of a computer. The movements of the bottom head were directed through software commands.

Figure 3.6. MTS machine with test assembly

3.3.5 Oscilloscope. An oscilloscope was used to adjust the corresponding voltage of the applied load from the load cell. It also helped conducting lead break tests to check the sensitivity of the bonded sensor when one is not interested to store data. A Lecroy LT344 Oscilloscope was used for this current research.

3.3.6 Fixture. A friction fixture, developed in the ISM lab, was used to conduct friction tests for the current research (Figure 3.7). With the help of this fixture, the bars were attached in the middle and the whole assembly was tightened by bolts.

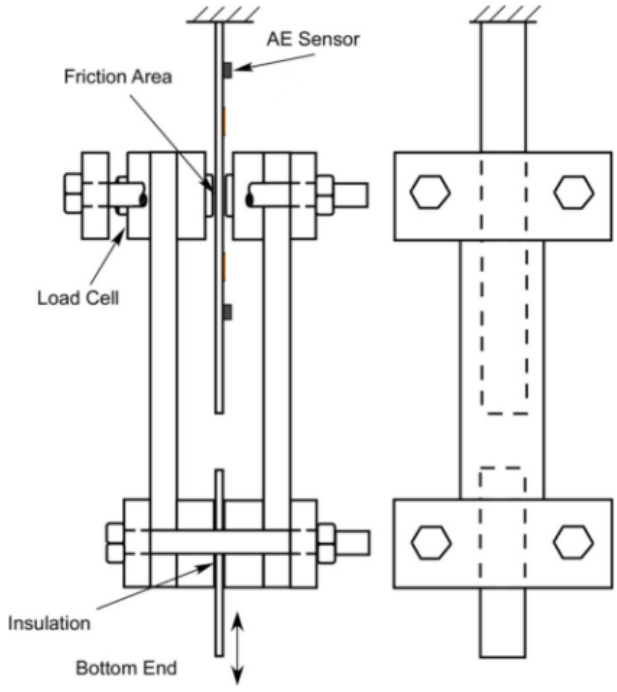

Figure 3.7. Schematic representation of the test fixture (Asamene and Sundaresan 2012).

3.4 Experimental Procedure

3.4.1 Sensor Bonding. A standard procedure, developed in the ISM lab, was followed during the bonding of the PZT sensor on the steel bar specimen. The electrode of the sensors was soldered with cables in order to connect them to the preamplifiers.

3.4.2 Lead Break Test. Before each friction test, a pencil lead break test was carried out to check the sensitivity of the bonded PZT sensor. The preamplifier gain was set to 40 dB for this test.

3.4.3 Test Control Parameters. The controlling parameters used in this research were:

- Normal pressure of 2 and 4 MPa nominal values.
- Sliding velocity (distance) of values 0.125, 0.25, and 0.5 mm/s
- Pairing of surfaces according to roughness
    i. Rough – rough (RR) pair of R_a value 1.5 µm and
    ii. Smooth – smooth (SS) pair of R_a value 0.6 µm.

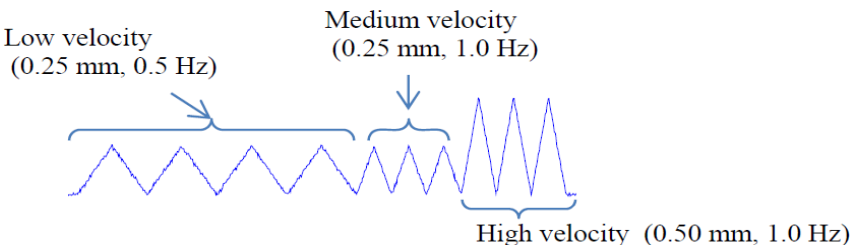

Figure 3.8. Test amplitude and frequency

The oscillation distances for different velocity tests are described in Figure 3.8. The amplitudes of travelling distances were same for low and medium velocity, but was double in case of high velocity tests. The pressure was adjusted by calculating the load and the corresponding voltage of the load cell (assuming a uniform pressure under the friction pad of 50 mm x 5 mm area). The varying parameters made twelve independent tests as follows in Table 3.1.

Table 3.1

Friction Test Combinations

Parameters	**Low velocity**	**Medium velocity**	**High velocity**
Smooth-Smooth	2 MPa	2 MPa	2 MPa
Smooth-Smooth	4MPa	4MPa	4MPa
Rough-Rough	2 MPa	2 MPa	2 MPa
Rough-Rough	4MPa	4MPa	4MPa

For each combination, a friction test for 3000 cycles was carried out. For each test, new pad and bar surfaces were used. The temperature and humidity were not controlled in this study. The same material was used for each test, so there was no possibility for changes in the hardness. Insulation was inserted in the mounting ends of the bar to avoid electrical noise. The signal parameters for the data acquisition setup are as follows in Table 3.2.

Table 3.2

Signal Acquiring Parameters

Sl. No	**Parameters**	**Value**
1	Amplification	60 dB
2	Threshold	30 dB (except R2 high, S2 medium,S2high 35dB)
3	Sample rate	10 Msps
4	HDT	600 µs
5	PDT	300 µs
6	HLT	1000 µs

3.5 Data Processing

3.5.1 Data Acquisition Setup. The AE signals generated on the friction surface and collected by the sensors were received and recorded by a PCI-2 data acquisition system. This system had the ability to store a wide range of parameters from the waveforms. The signal acquiring parameters and internal amplification were defined in AE-win software. The waveforms generated from the original data files were created by the same software.

Figure 3.9. PCI-2 data acquisition setup

3.5.2 Data Analysis. The signals received by the data acquisition system contained noise data. We filtered them with Matlab® codes developed by ISM lab members. The analysis of the waveforms was done by Noesis™ 5.2 software. The frequency components in each signal were analyzed by the Agu-Vallen Wavelet™ software.

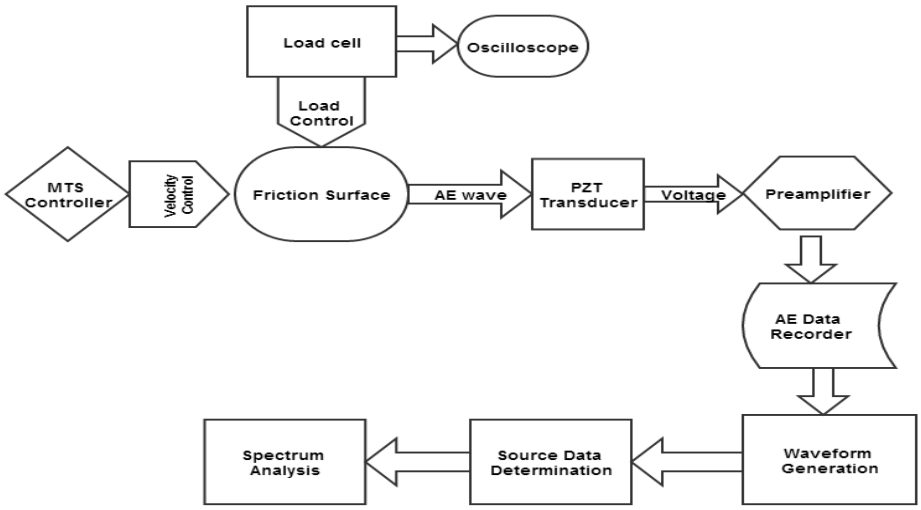

Figure 3.10. Experiment flow chart

3.5.3 Source Location Determination. To avoid noise signals in the analysis, a source location identification method was used. The maximum time difference between the signals received by sensor1 and sensor2 was calculated. This was performed by measuring the maximum difference from the sensor to friction surface distance and using the sound velocity in steel (Appendix A). The signals which are received by both sensors within a time period are coming from friction area. The calculation of differential time can be performed as following

For, Friction distance from Sensor1=d1 &

Friction distance from Sensor2=d2

Maximum Differential Distance, $\Delta d = |d1-d2|$

Differential Time, $\Delta t = \Delta d/v$, where v= Velocity of sound in the plate

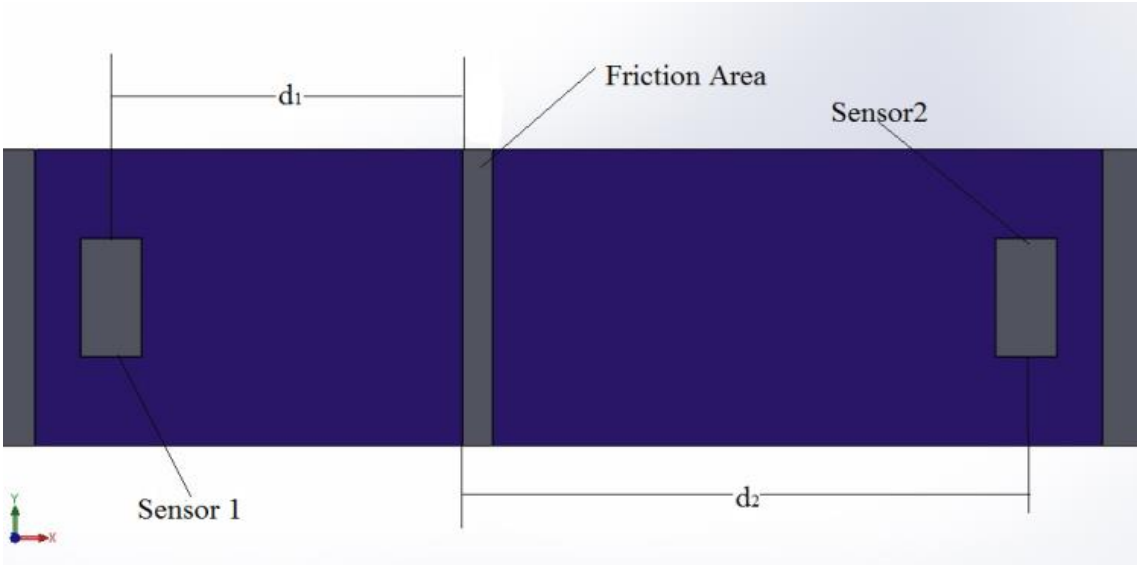

Figure 3.11. Source location determination technique

Table 3.3

Source Location Chart

Sl No	Test	Sensor1 Distance, mm	Sensor2 Distance, mm	Maximum Difference, mm	Time Difference Considered, µs
1	Smooth-2 MPa-Low	105	47	58	12
2	Smooth-2 MPa-Medium	93	59	34	8
3	Smooth-2 MPa-High	85	71	14	3
4	Rough-2 MPa-Low	120	57	63	13
5	Rough-2 MPa-Medium	107	70	37	8
6	Rough-2 MPa-High	98	80	18	4
7	Smooth-4 MPa-Low	82	70	12	3
8	Smooth-4 MPa-Medium	91	61	30	6
9	Smooth-2 MPa-High	49	103	54	11
10	Rough-2 MPa-Low	69	109	40	8
11	Rough-4 MPa-Low	57	92	35	7
12	Rough-4 MPa-Low	57	121	64	13

3.6 Damaged Surface Analysis

3.6.1 Measurement of Roughness Change. For measuring the roughness of the undamaged and damaged surfaces, a WYKO (Model 95) surface profiler was used. The maximum measurable topography for this machine is 1 mm.

Figure 3.12. Surface profiler

3.6.2 Microscopic Imaging of Damaged Surface. A ZEISS Imager M2M AX10 was used to characterize the topography of the damaged surfaces after friction tests. 50 x zoom was used to take images of every friction area.

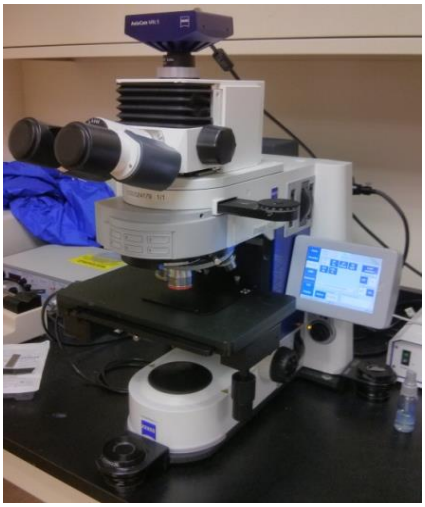

Figure 3.13. Optical microscope

CHAPTER 4

Results & Analysis

4.1 Introduction

When a surface is sliding over another surface under a normal pressure, the force exerted on them can create changes in crystal structures either elastically or plastically. Any change in structure may create stress waves that propagate in the form of sound waves or AEs. Detection of AEs depends on (i) how much amplification of the signals we are getting after reception by the sensors and (ii) the choosing of the threshold value for avoiding noise signals. Most of the previous authors, such as (Hase, Wada et al. 2008), acquired signals from the plastic deformation and wear of materials. The elastic collision may occur at very low amplitude where wear may not present. The performance of the sensor plays an important role for detecting this type of signal. Along with microscopic images, change of surface roughness values found in this study is described in this chapter. The wear type of the damaged surface is also predicted The details of surface wear found will be analyzed later in this chapter.

4.2 Comparison of AE at Different Velocities

The maximum axial loads observed for different tests are listed in Table 4.1. The trend found in Table 4.1 is the rise in velocity increased the amount of maximum axial load in the friction tests. The trend of axial load exerted by the friction surfaces is unambiguous. The rise in velocity led to a rise in axial forces and, hence, friction coefficients. It was expected that the rise in friction coefficients would create more AEs.

The AE events are shown in Figure 4.1. The figure suggests that most of the AE events were found in the gross slip of the surfaces (in their peak values). Mixed slip (partial and gross) events were found more in the high velocity tests and were very minimal or absent during both

low and medium velocity tests. AE signals from mixed slip events occurred within amplitude bands of about 30 to 50 dB. The AE events of amplitudes above 50 dB occurred mostly at the slip of peak loads. Another clear observation is that high amplitude (more than 50 dB) signals were more common in higher velocity tests. The peak load for higher velocity tests was also significantly higher.

Table 4.1

Maximum Axial Load in Newton for Different Tests

Test	Low	Medium	High
R2	714	750	815
S2	665	620	910
S4	1180	1370	1435
R4	1090	1411	1510

Figure 4.1 also indicates a uniform amplitude distribution over a range of 30 dB to 50 dB with a higher percentage of events in the range of 30 to 40 dB (or 35 to 40 dB depending on the threshold setting). Some high amplitude events, as well as some low amplitude events, at higher velocity were present which indicates a wider range of amplitudes at high velocity.

Figure 4.2 suggests that the cumulative events and cumulative absolute energy gain characteristics were similar for lower velocities. However, at higher velocities, a noticeable increase of events and energy for the same travelling distances were found. The fluctuation of event rate of the first two graphs, that was not common in the high velocity case, is probably because of the higher volume of events at higher velocity.

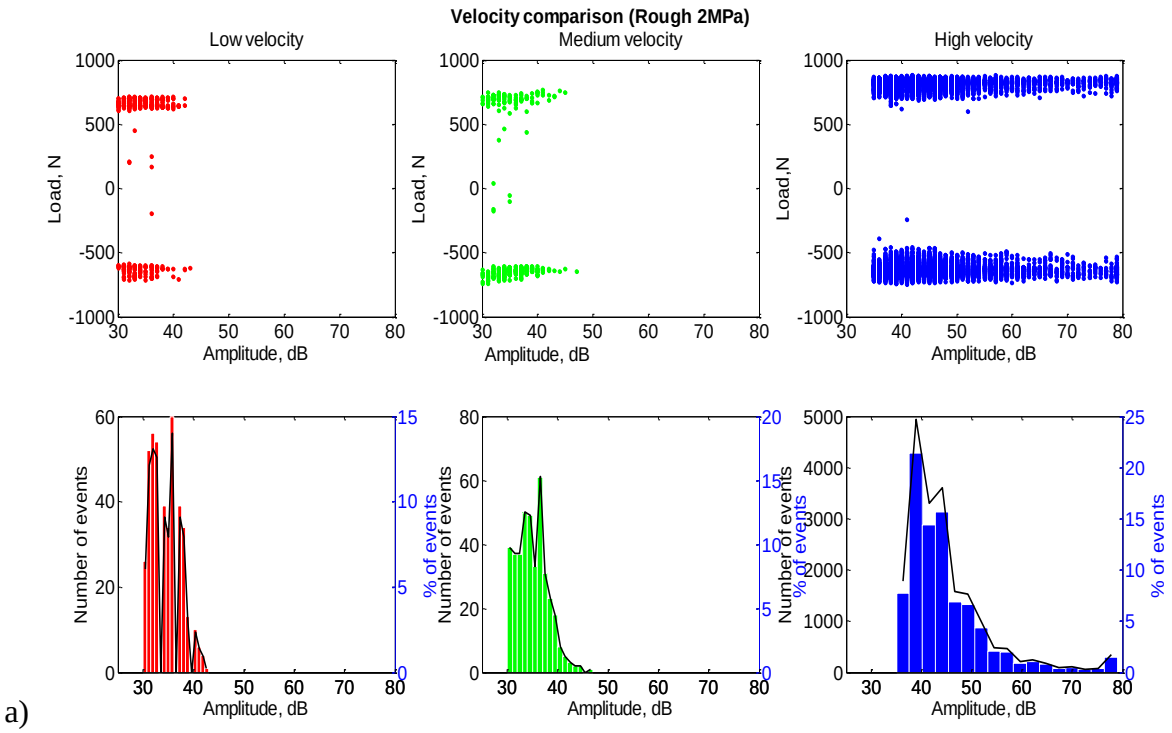

a)

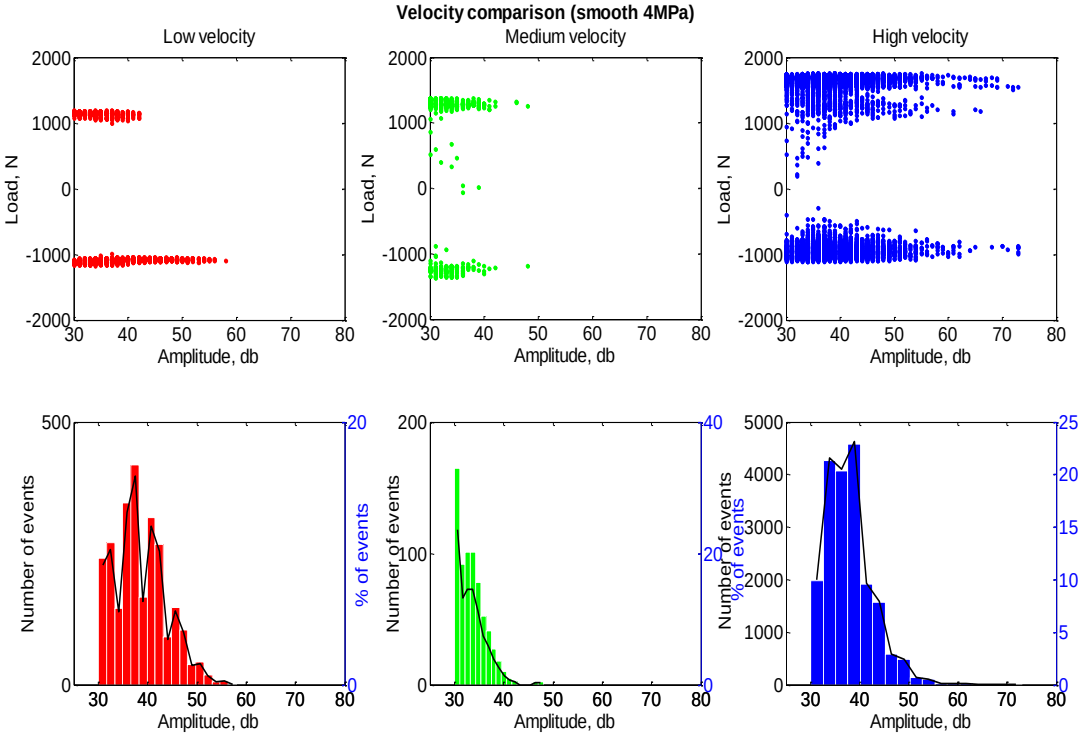

b)

Figure 4.1. Amplitude distributions of different velocity AE events for

a) Rough-rough low pressure combinations

b) Smooth-smooth high pressure combinations

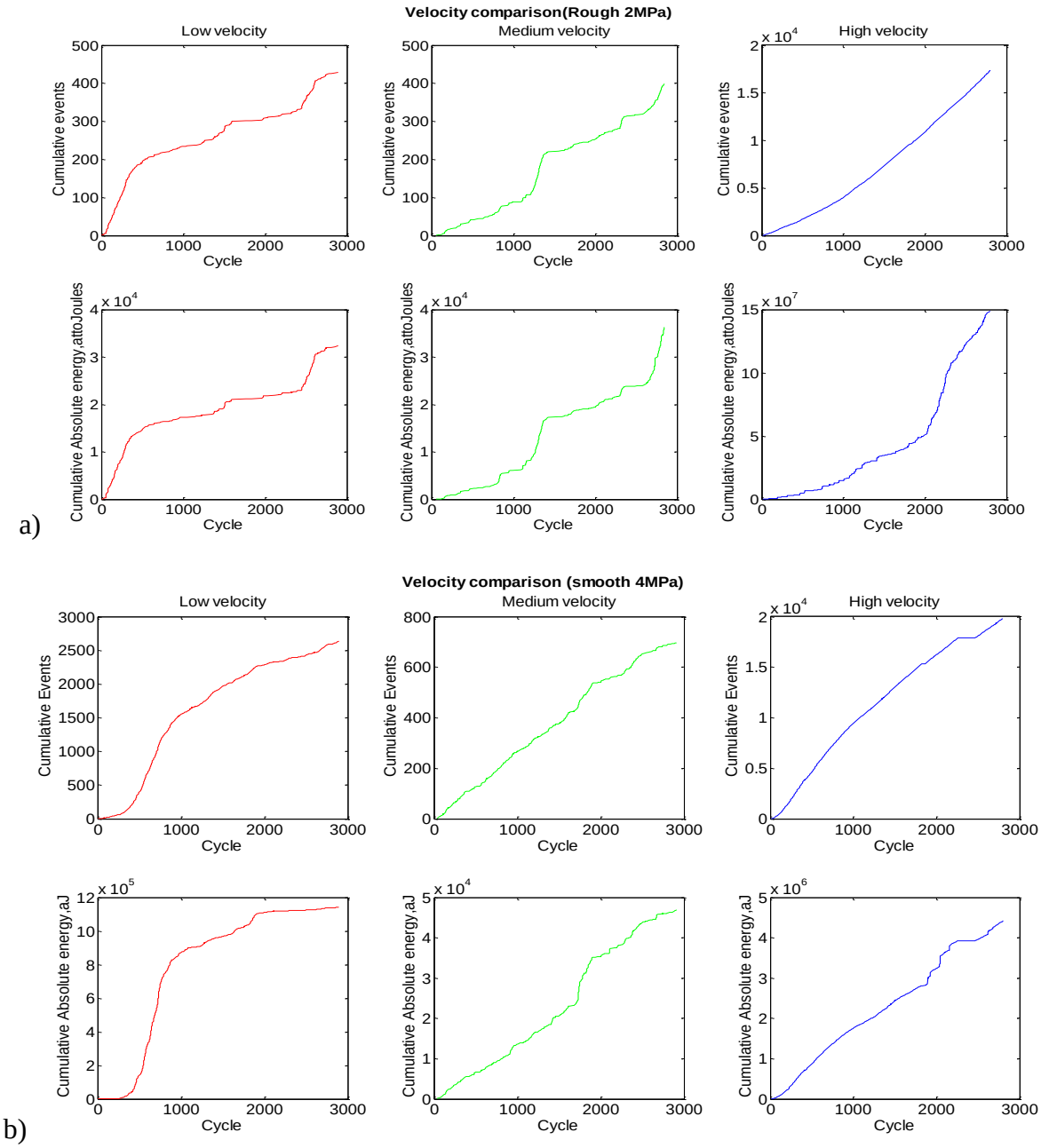

Figure 4.2. Cumulative events & AE energy at different velocities

a) Rough-rough low pressure combinations

b) Smooth-smooth high pressure combinations

Allover the tests of rough case (Figure 4.2a), a sharp increase of AE events per cycle was almost regular observed. For the smooth case, a sharp increase in the number of events, as well as the AE energy, occurred only in the low velocity test after around 400 cycles (Figure 4.2b).

4.3 Comparison of AE at Different Roughness

In the comparison of the cumulative number of events and the cumulative absolute energy of different tests, it is seen, in the case of low velocity, the initial trend for rough surfaces registered a higher number of events. As the number of cycles or sliding distance increased, the number of events for the smooth surfaces became higher.

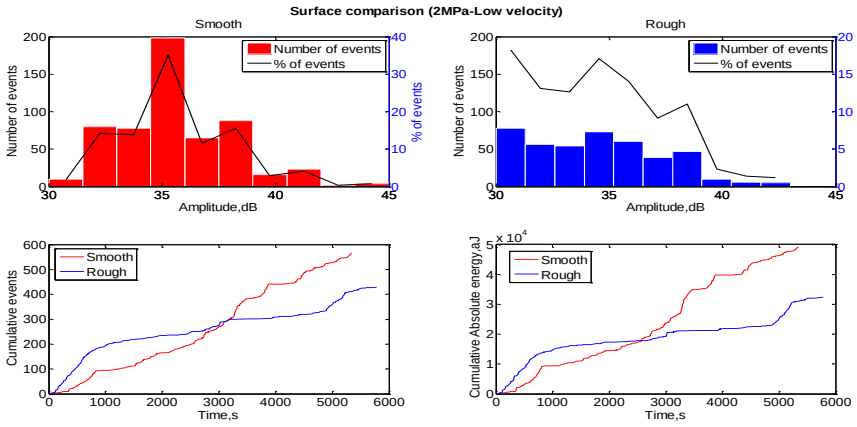

Figure 4.3. Comparison of Surface roughness on AE at low velocity (at 2 MPa pressure)

i. Amplitude and event distribution (top two graphs)

ii. AE events vs. time (bottom two graphs)

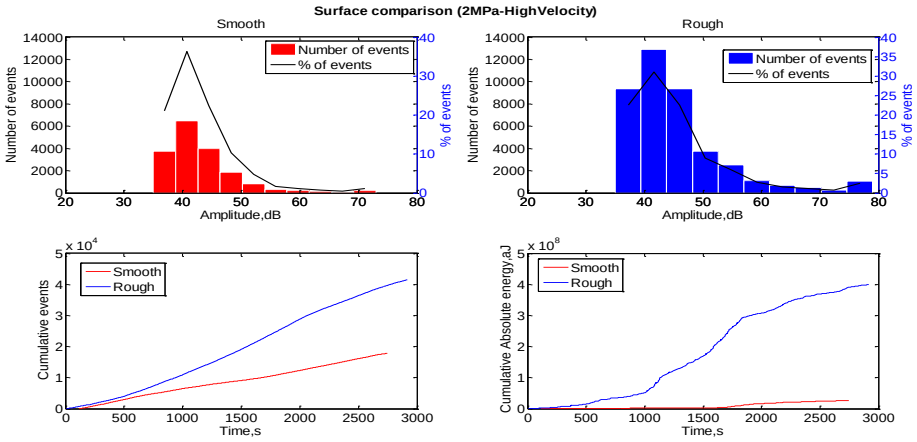

Figure 4.4. Comparison of Surface roughness on AE at high velocity (at 2 MPa pressure)

i. Amplitude and event distribution (top two graphs)

ii. AE events vs. to time (bottom two graphs)

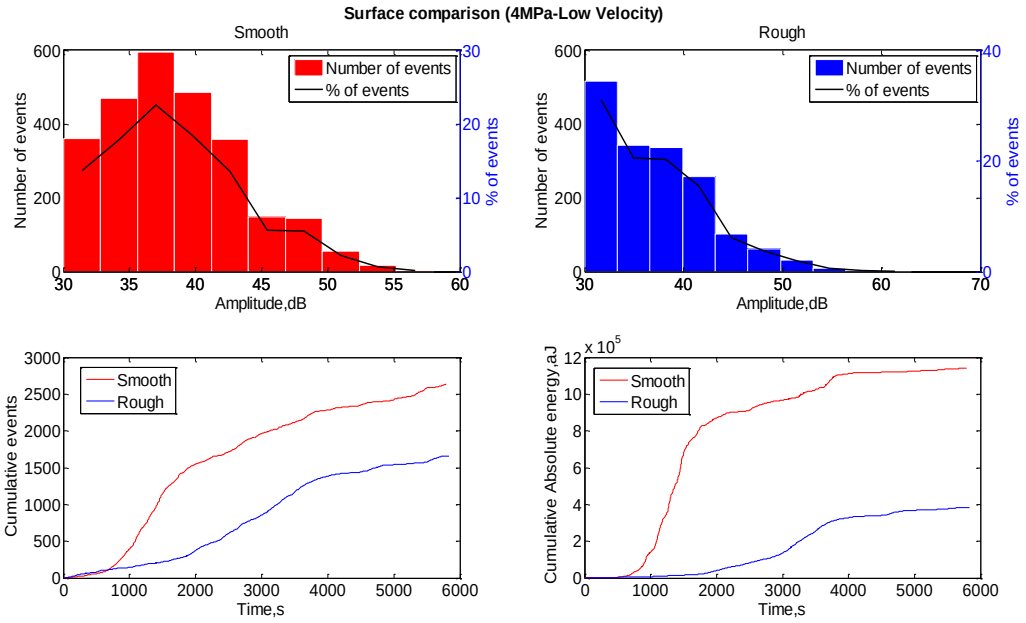

Figure 4.5. Comparison of Surface roughness on AE at low velocity (at 4MPa pressure)

i. Amplitude and event distribution (top two graphs)

ii. AE events vs. time (bottom two graphs)

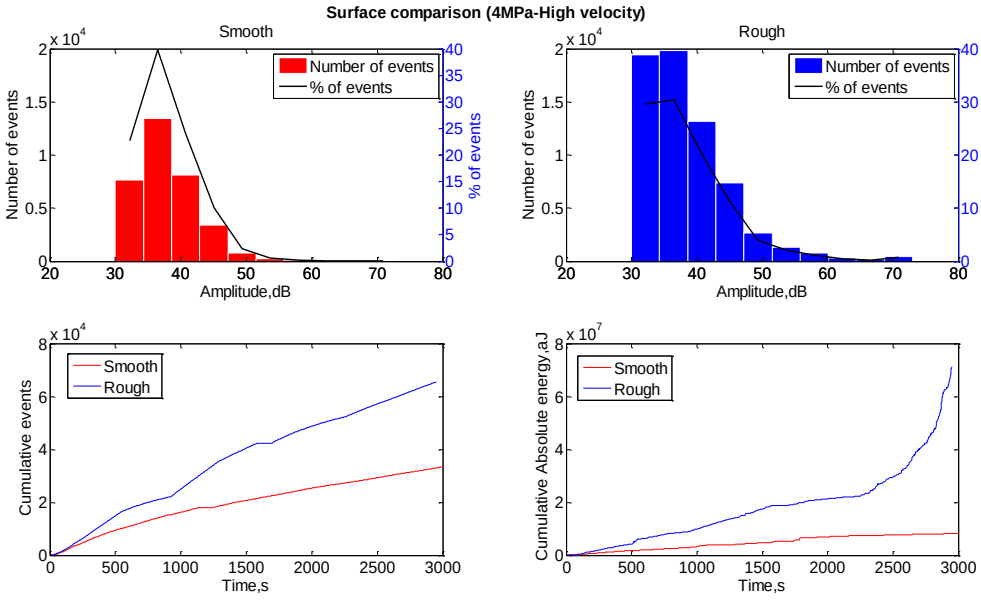

Figure 4.6. Comparison of Surface roughness on AE at high velocity (at 4MPa pressure)

i. Amplitude and event distribution (top two graphs)

ii. AE events vs. time (bottom two graphs)

In both cases (2 MPa and 4 MPa tests) for low velocity tests, smooth surfaces gave more AEs. For high velocity tests (Figure 4.4 & 4.6), the rough combination had a higher number of events and cumulative absolute energy. The high velocity also gave an increase of high amplitude events.

4.4 Comparison of AE at Different Normal Pressures

The amplitude distribution with number of events, cumulative events, and cumulative energy trend with respect to time at different load levels are described in Figures 4.7 to 4.10 for the smooth pair surface cases. For low velocity, the amplitude range and cumulative energy were found to be larger in high pressure cases.

The variations of cumulative energy were found to be different in each case. For low velocity (Figure 4.7 & 4.9), the rise of AE energy was similar to the number of events. The change of AE events and energy was exponential (up to 2000 s) for the 4 MPa test, but was linear throughout the 2 MPa test.

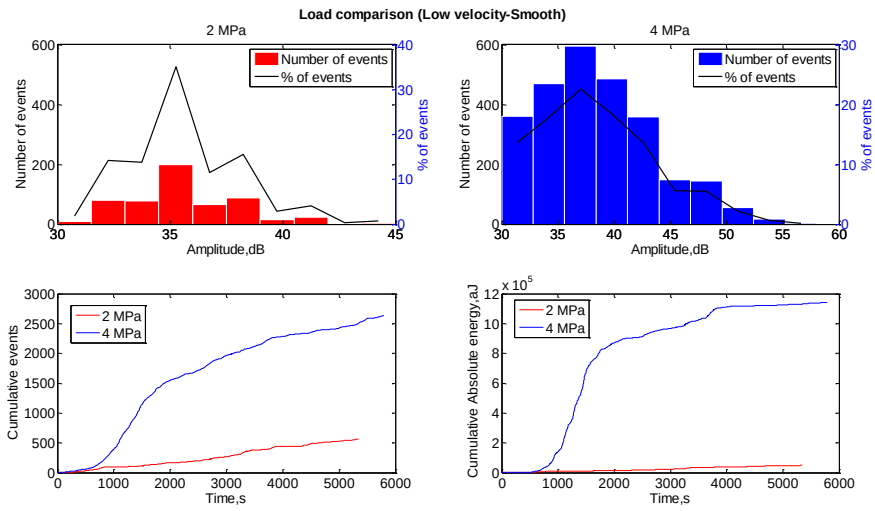

Figure 4.7. Comparison of normal load on AE at low velocity (for smooth surface pairs)

i. Amplitude and event distribution (top two graphs)

ii. AE events with respect to time (bottom two graphs)

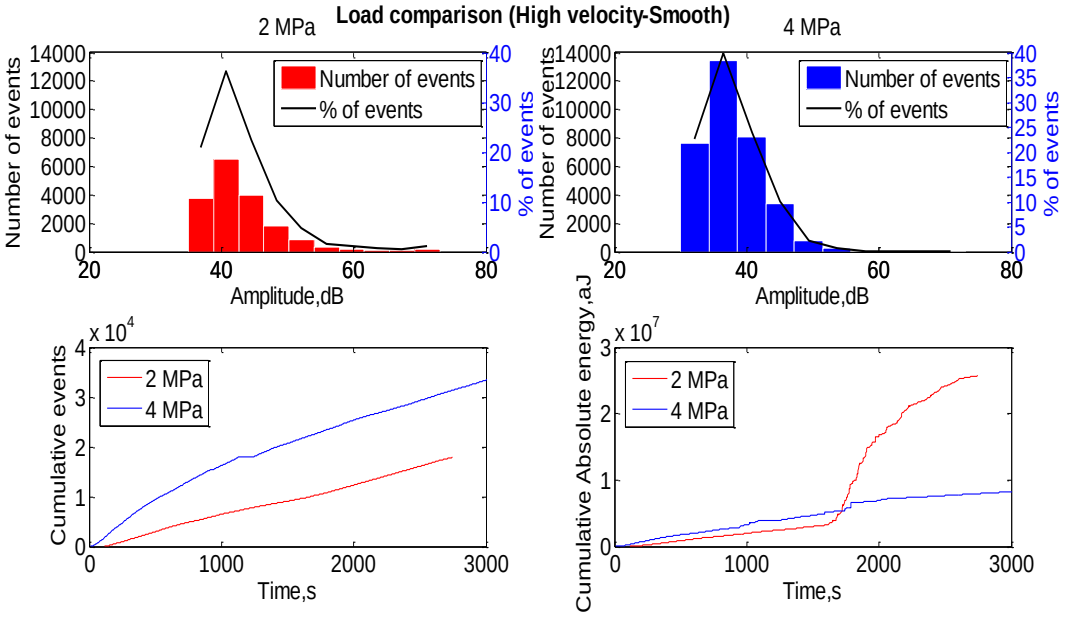

Figure 4.8. Comparison of normal load on AE at high velocity (for smooth surface pairs)

i. Amplitude and event distribution (top two graphs)

ii. AE events & energy with respect to time (bottom two graphs)

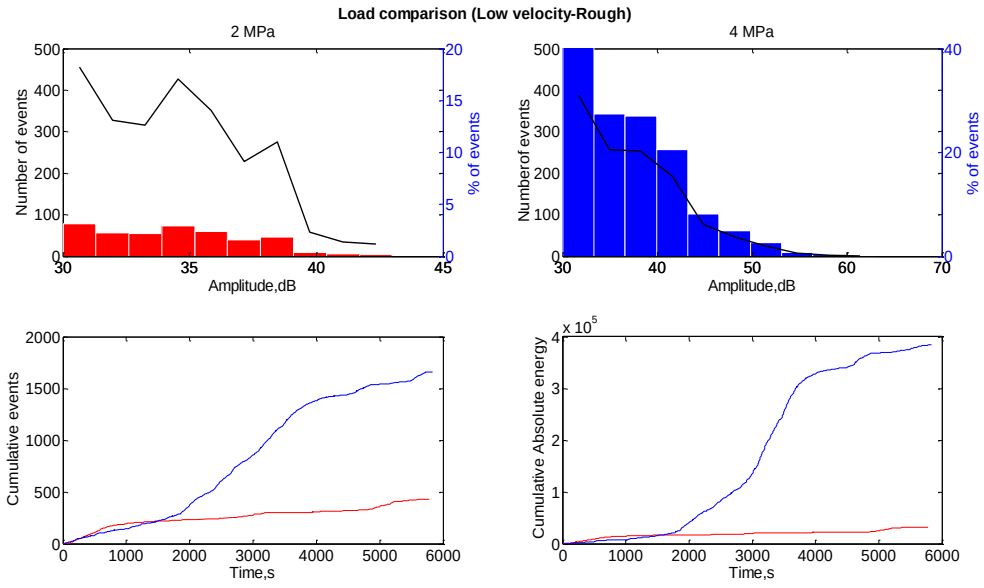

Figure 4.9. Comparison of normal load on AE at low velocity (for rough surface pairs)

i. Amplitude and event distribution (top two graphs)

ii. AE events & Energy with respect to time (bottom two graphs)

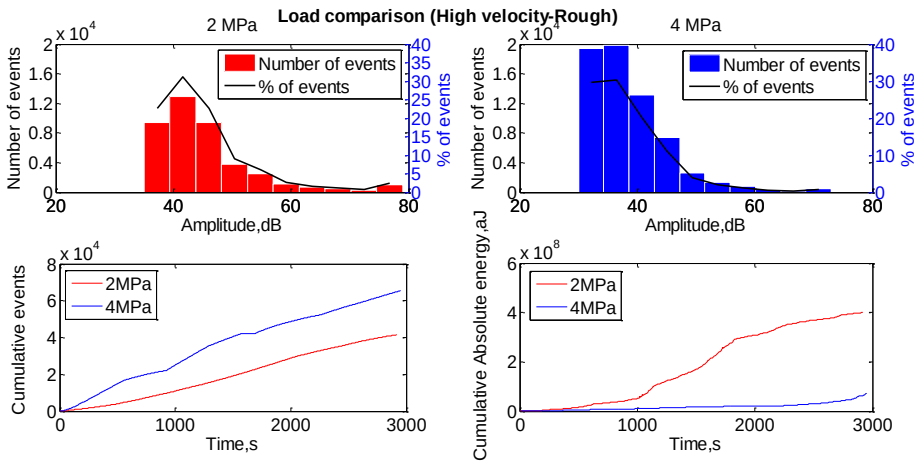

Figure 4.10. Comparison of normal load on AE at High velocity (for rough surface pairs)

i. Amplitude and event distribution (top two graphs)

ii. AE events & energy with respect to time (bottom two graphs)

For the high velocity case of smooth pair surfaces (Figure 4.7 & 4.8), the number of events of AE was always greater for the 4 MPa test. The AE events and energy increased sharply after 1700 cycles (1700s). The amplitude in this case had a wider distribution supporting its sudden energy change. The effect of changing normal load on AE for the high velocity rough pair tests (Figure 4.9 & 4.10) was slightly different in terms of events and AE energy. The 2 MPa test gave more AE energy than the 4 MPa test, though the number of events was less. It indicates that some hits with larger amplitudes were missed by the detection system in the 4 MPa test. The discrepancy was a result of setting different threshold values for the two tests. For 2 MPa test the threshold value was 35 dB whether for 4 MPa test it was 30 dB. The data acquisition system for each case was supposed to receive the first signal it encountered. If a signal of 30 dB amplitude was received it waited 1000 micro seconds to take another signal. So, If there comes another signal of more than 30 dB amplitudes after few microseconds of the signal the data acquisition system was unable to record that. It created a situation that many larger amplitude signals might not be recorded in case where threshold is low.

4.5 Variation of Waveform

4.5.1 Variation of Waveform within a Test. The frequency spectrum within a signal for the 2 MPa rough pair high velocity test is presented in Figures 4.11 to 4.14. Each signal had an amplitude of 38 dB. Dispersion curves for a 3 mm steel plate were superimposed on the same figure. In each graph along the horizontal axis, time was counted in microseconds. From the wavelet images, the two basic modes of Lamb waves are evident.

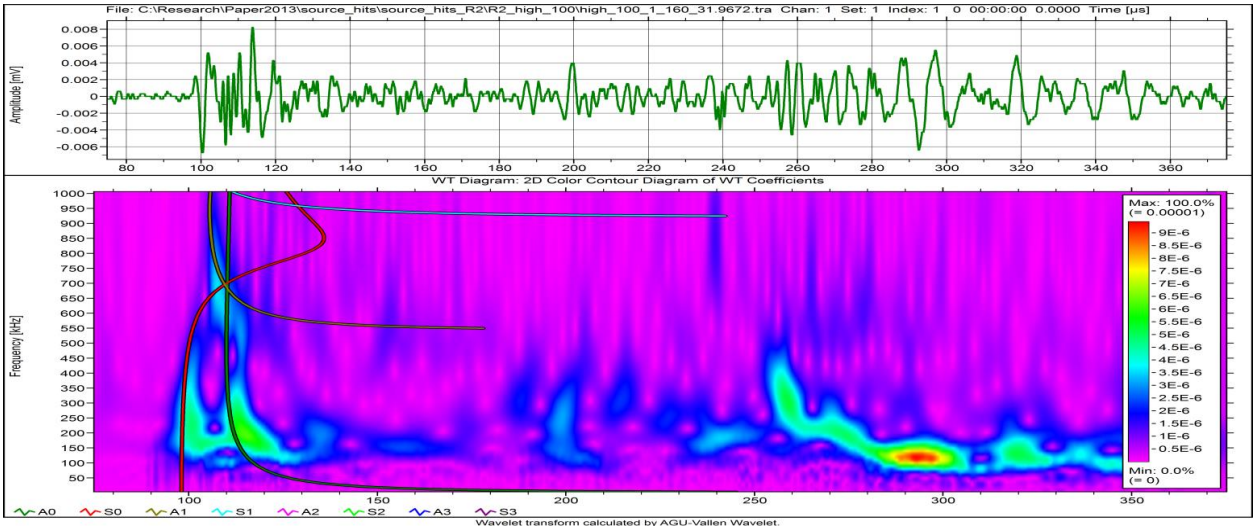

Figure 4.11. Waveform of high velocity rough pair 2 MPa test after30 cycles

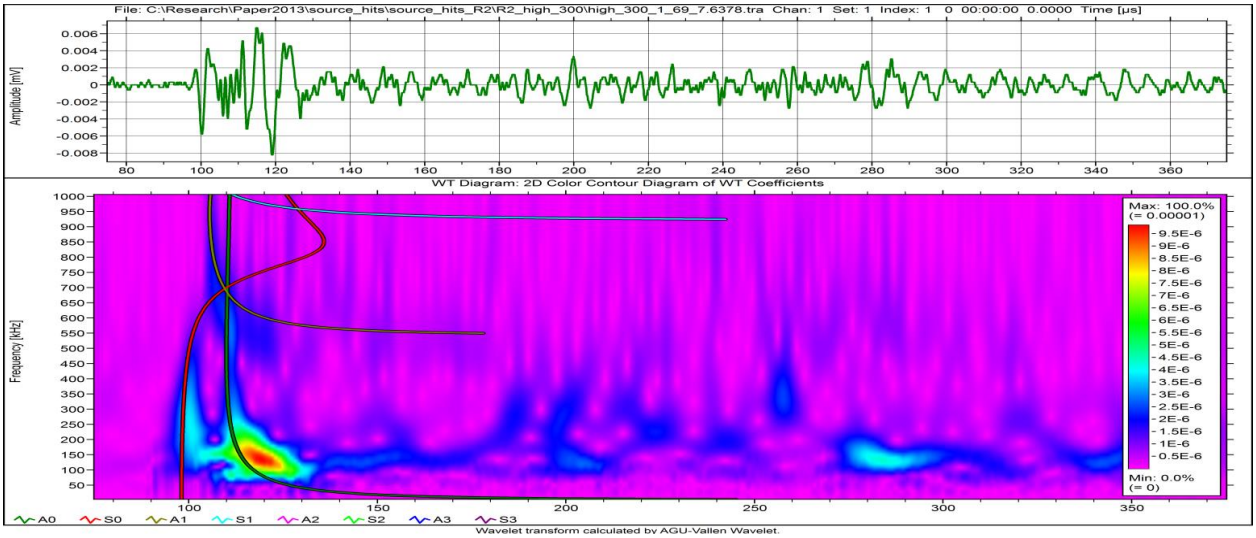

Figure 4.12. Waveform of high velocity rough pair 2 MPa test after 169 cycles

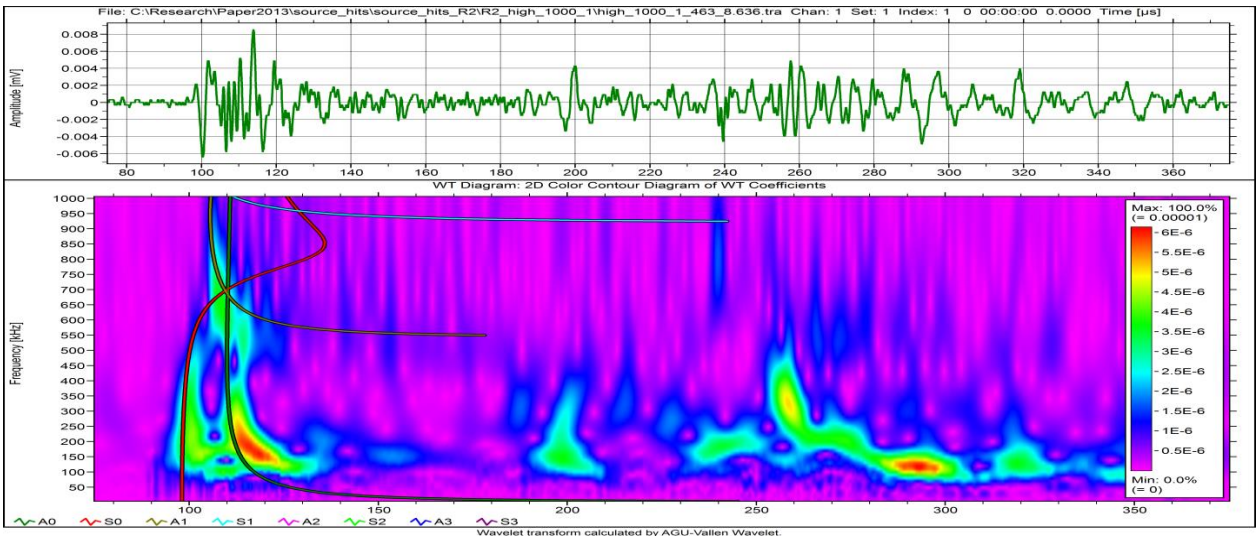

Figure 4.13. Waveform of high velocity rough pair 2 MPa test after 808 cycles

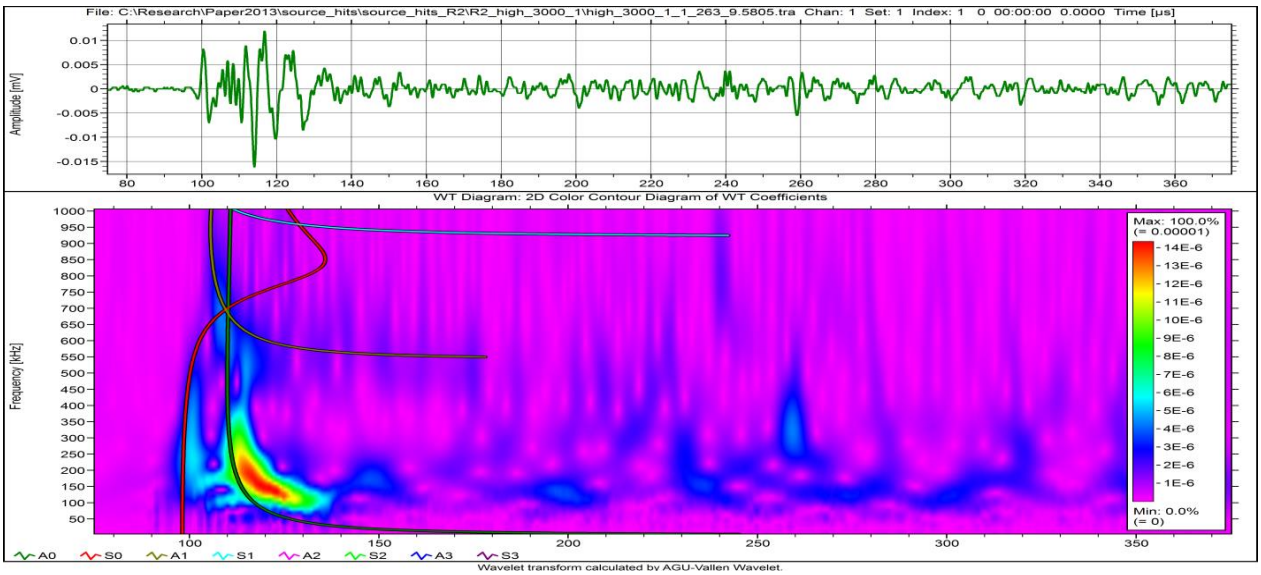

Figure 4.14. Waveform of high velocity rough pair 2 MPa test after 2009 cycle

The frequency components for different signals in a particular test are similar in nature. They varied in range from 100 kHz to 1 MHz, but the most intensity was found in 100 to 400 kHz. The dominance of the anti-symmetric component over the symmetric component in the waveform is also evident, and this increases with time (from 100 cycles to 3000 cycles). The A_1 mode is also present in the waveform at around 650 kHz. The anti-symmetric mode becomes clearer after around 200 cycles of the test.

4.5.2 Variation of Waveform with Changing Velocity. The 2 MPa smooth pair tests were considered to compare waveforms at different velocities. Each waveform was taken at a 38 dB amplitude. The waveforms were selected after 1000 cycles of the tests. For low velocity test, most of the frequency components were less than 450 kHz (Figure 4.15). In each graph along the horizontal axis, time was counted in microseconds.

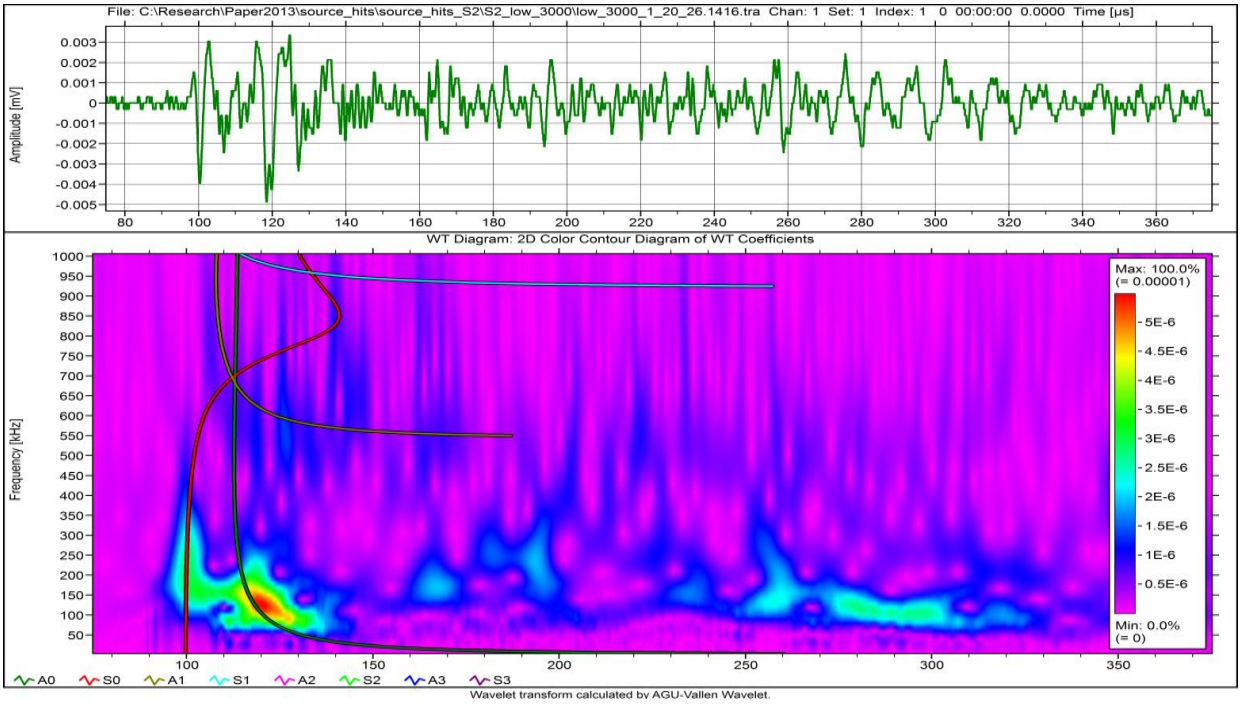

Figure 4.15. Waveform of low velocity smooth pair 2 MPa test

The trend in the change of the waveform with the changing velocity is evident by its frequency spectrum. By increasing the velocity (Figure 4.16 & 4.17), the possibility of getting high frequency components in a signal increases more. The low velocity A_1 component was almost absent. The range of frequency also increased from 100-350 kHz to 100-450 KHz. By high frequency components, it is referred to the frequency spectrum of more than 500 KHz.

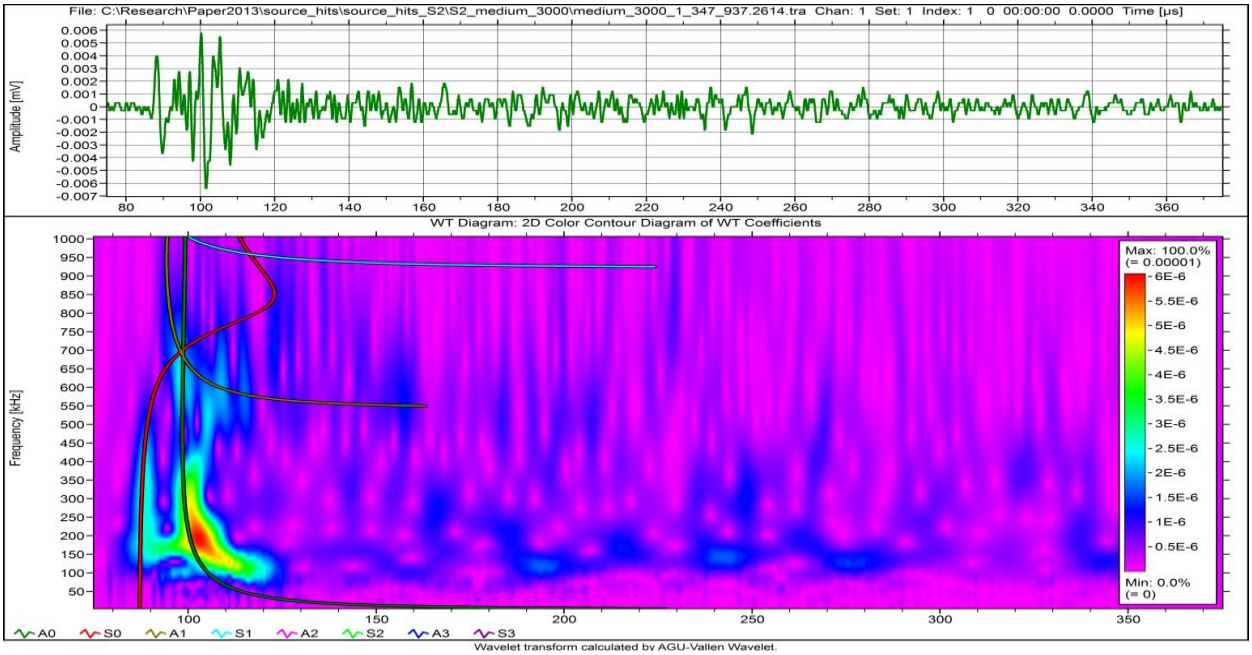

Figure 4.16. Waveform of medium velocity smooth pair 2 MPa test

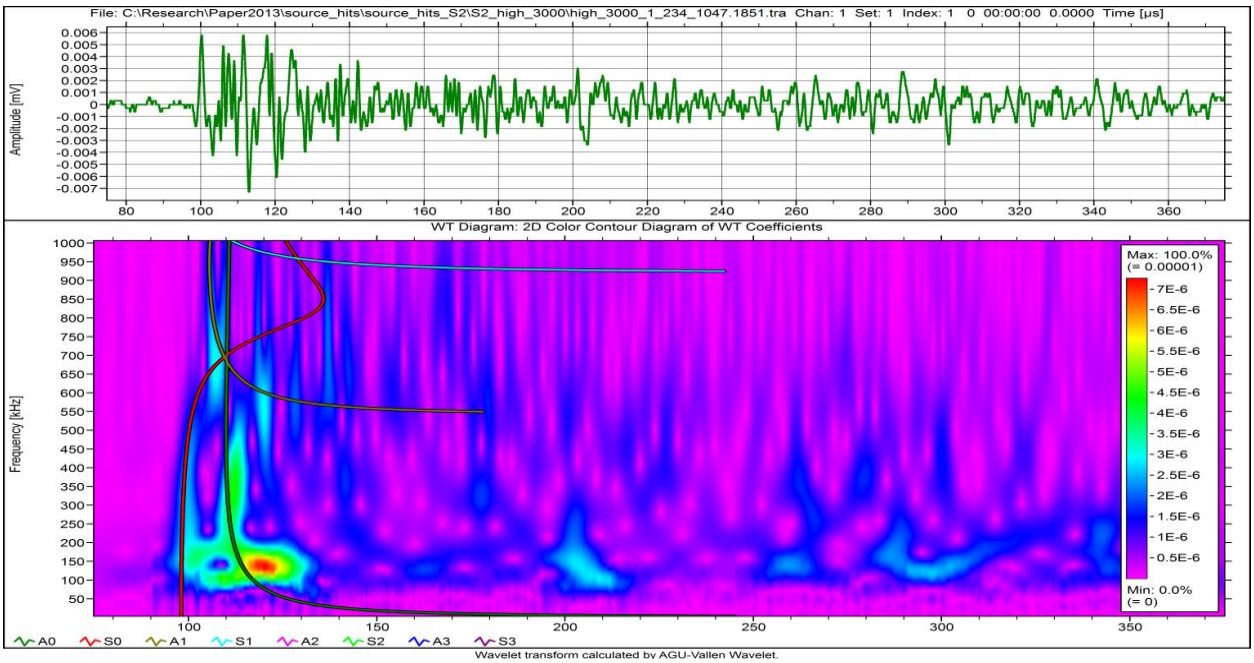

Figure 4.17. Waveform of high velocity smooth pair 2 MPa test

For the higher velocity tests, the anti-symmetric modes of the waveforms were more evident (Figure 4.16 & 4.17). The presence of the A_1 mode for the higher velocity is also a clear feature.

4.5.3 Variation of Waveform with Changing Roughness. The 2 MPa medium velocity and low velocity 4MPa tests to compare waveforms at different velocities (Figure 4.18 to 4.21). All the wavelet images were taken at a 38 dB amplitude value. The waveforms were taken after 1000 cycles of tests. In each graph along the horizontal axis, time was counted in microseconds.

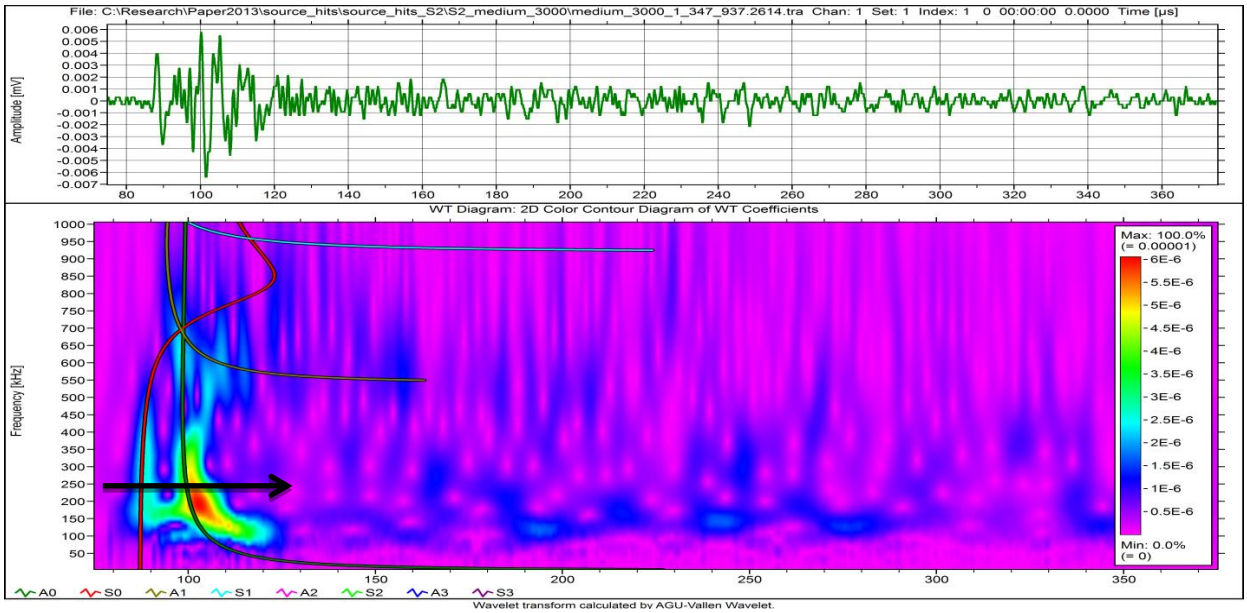

Figure 4.18. Waveform of medium velocity smooth pair 2 MPa test

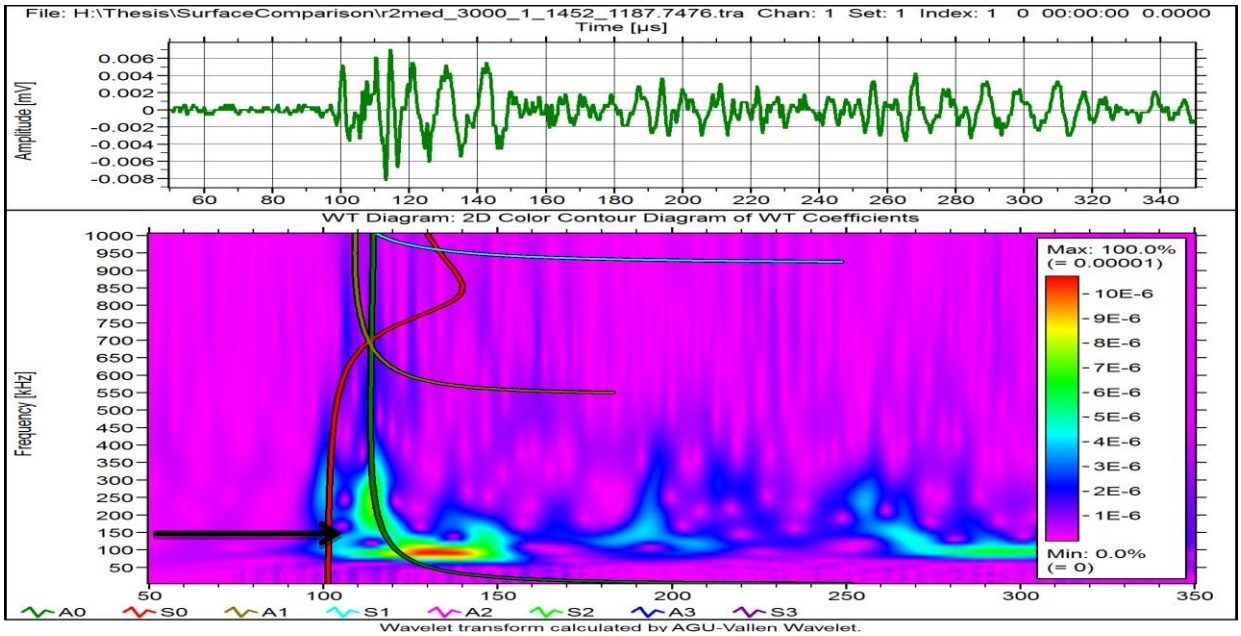

Figure 4.19. Waveform of medium velocity rough pair 2 MPa test

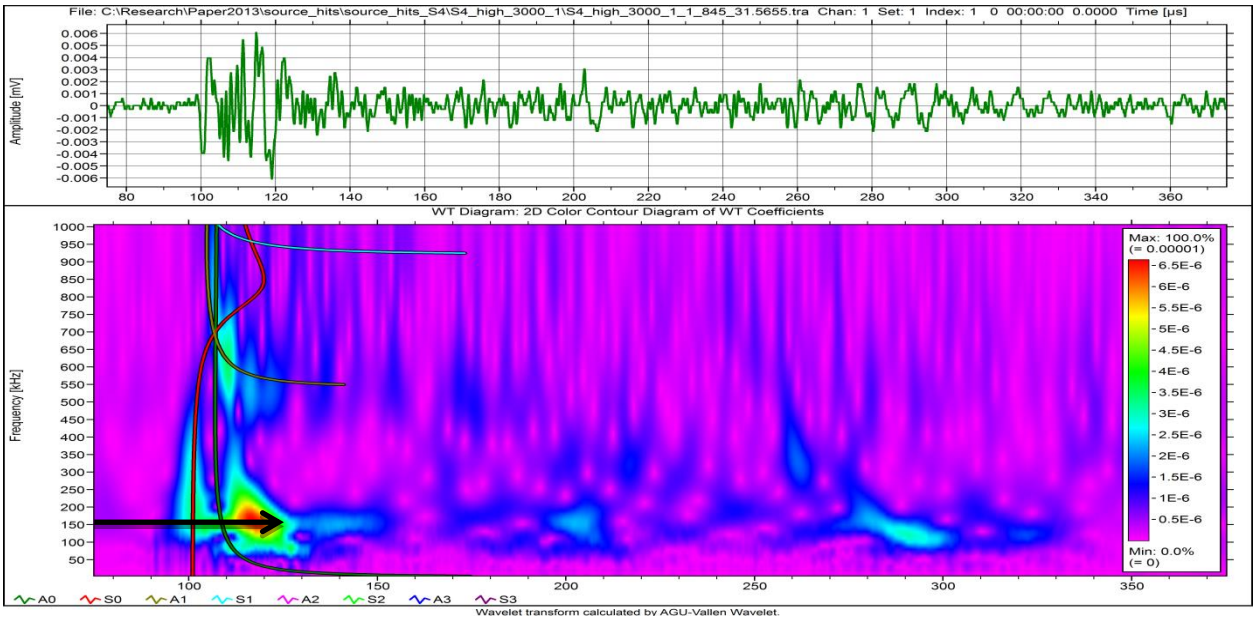

Figure 4.20. Waveform of high velocity smooth pair 4MPa test

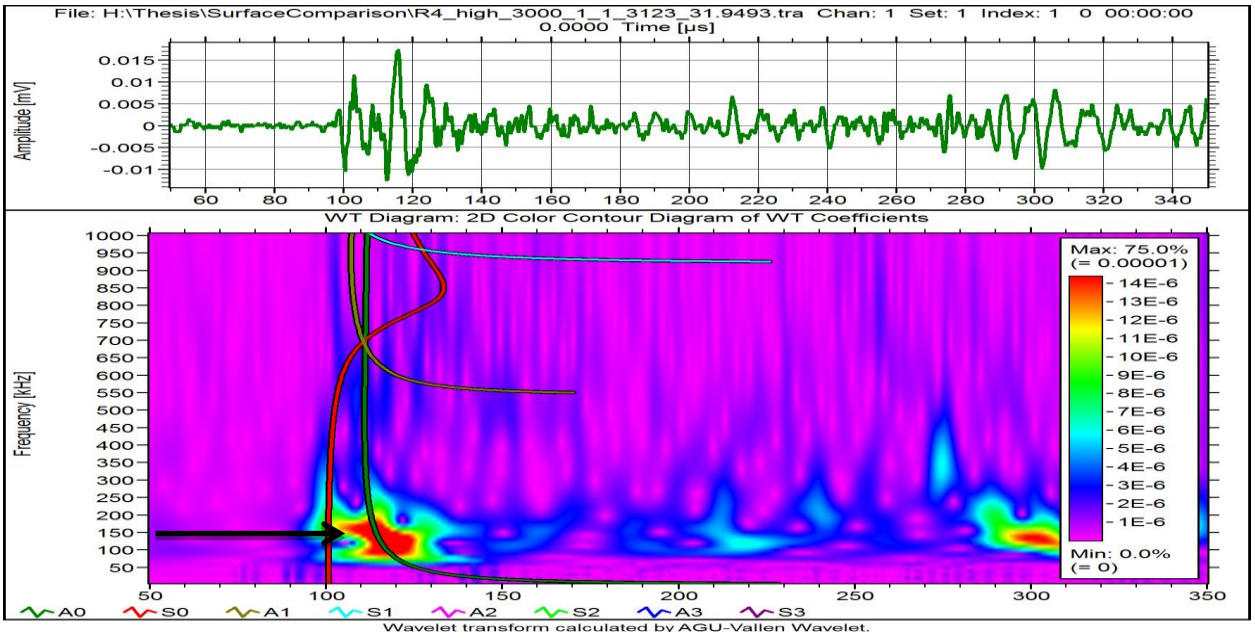

Figure 4.21. Waveform of high velocity rough pair 4MPa test

The variation of waveforms for changing the roughness (Figure 4.18 to 4.21) gave a clear indication of the effect of surface roughness on AE signal waveforms. The frequency components for the smooth case were found to be higher than the rough case in both the 2 MPa and 4 MPa tests.

4.5.4 Variation of Waveform with Changing Normal Pressure. For comparing the wavelet images to observe the effect of the normal pressure on AE two pairs of tests were considered. For low velocity, rough pairs at a 34 dB amplitude and high velocity smooth pairs at 38 dB were taken. In each graph along the horizontal axis, time was counted in microseconds.

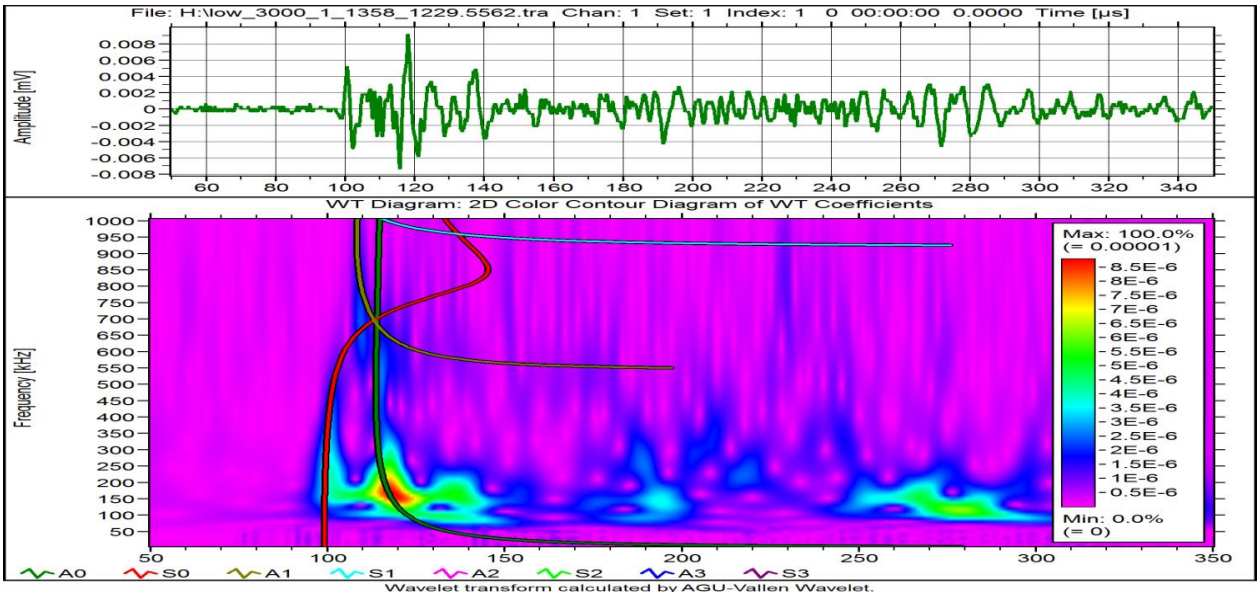

Figure 4.22. Waveform of Low velocity rough pair 2 MPa

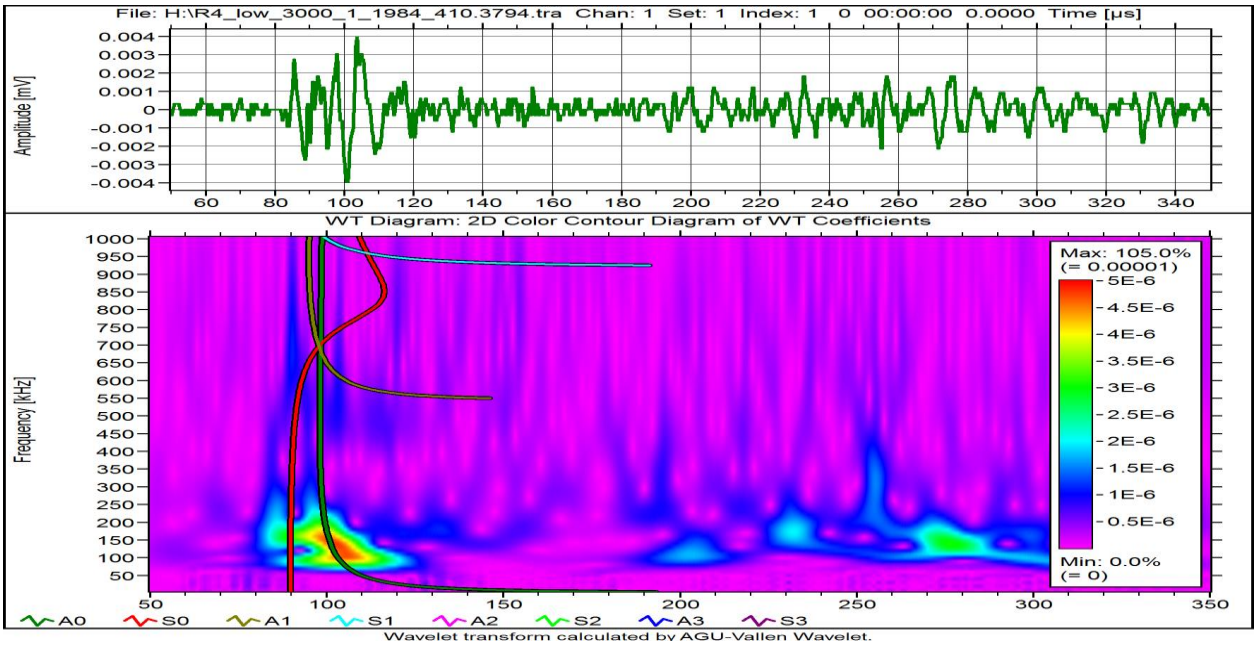

Figure 4.23. Waveform of Low velocity rough pair 4MPa test

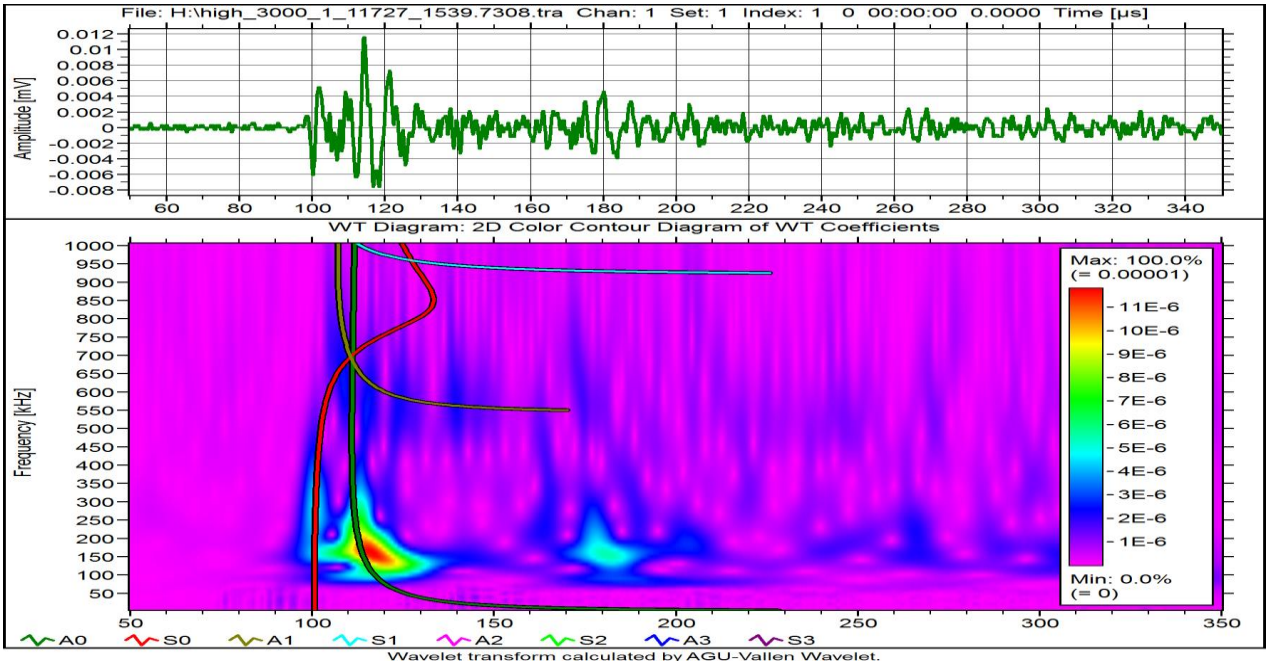

Figure 4.24. Waveform of High velocity smooth pair 2 MPa test

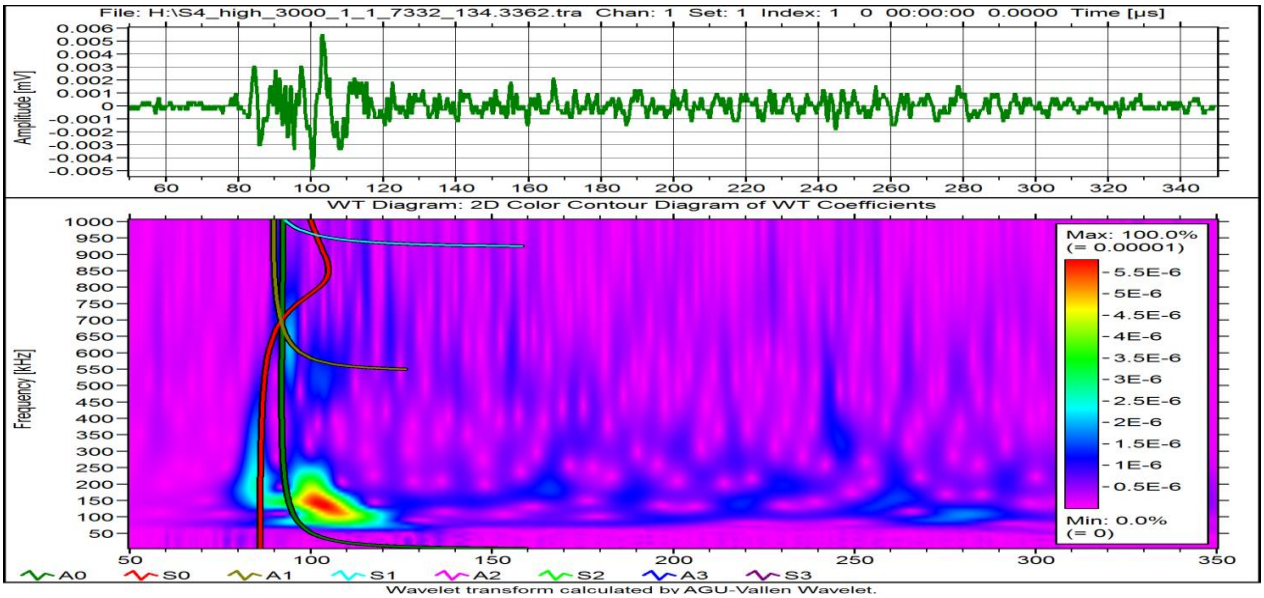

Figure 4.25 Waveform of High velocity smooth pair 4MPa test

The high frequency components for the rough 2 MPa test were more than the 4MPa test (Figure 4.22 & 4.23). For smooth cases (Figure 4.24 & 4.25), it was found that the 4MPa test gave more high frequency components than the 2 MPa test. It is apparently giving two contradictory results based on the dependence of the normal pressure on AE signal waveforms.

4.6 Observation of Change in Surface Topography

The surface prepared for friction test for the smooth case (Figure 4.26) and the change in surface topography after running a test of 3000 cycles for 2 MPa (Figure 4.27) gave a qualitative idea of the plastic degradation of the material due to friction. All the images were taken at 50 x magnification.

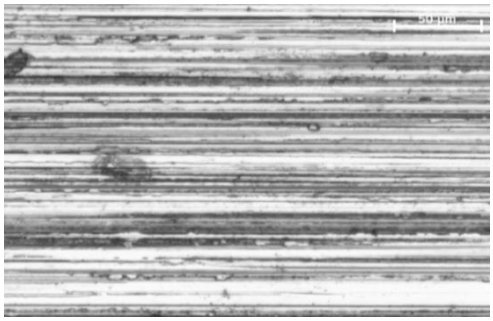

Figure 4.26. Undamaged smooth surface

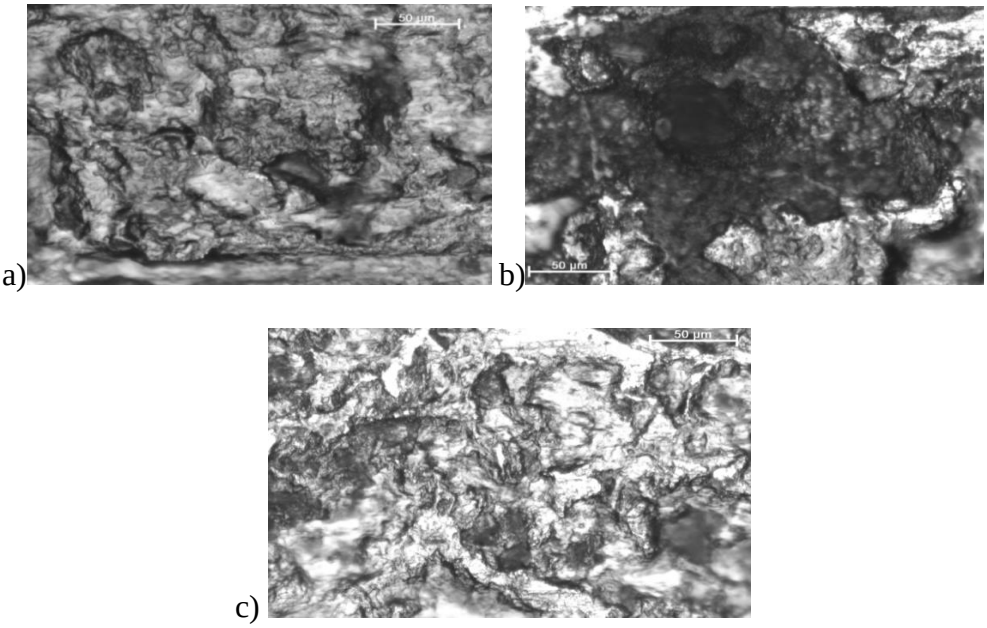

Figure 4.27. Effect on smooth surface-2 MPa normal pressure after 3000 cycle

a) Low velocity,

b) Medium velocity,

c) High velocity

The low velocity test (Figure 4.27) gave more wear than the high velocity test. For the medium velocity test, the surface damage as seen in the figures was the deepest. The wear type seen in these images was an irregular type and the existence of corrosion was evidenced by the black spots.

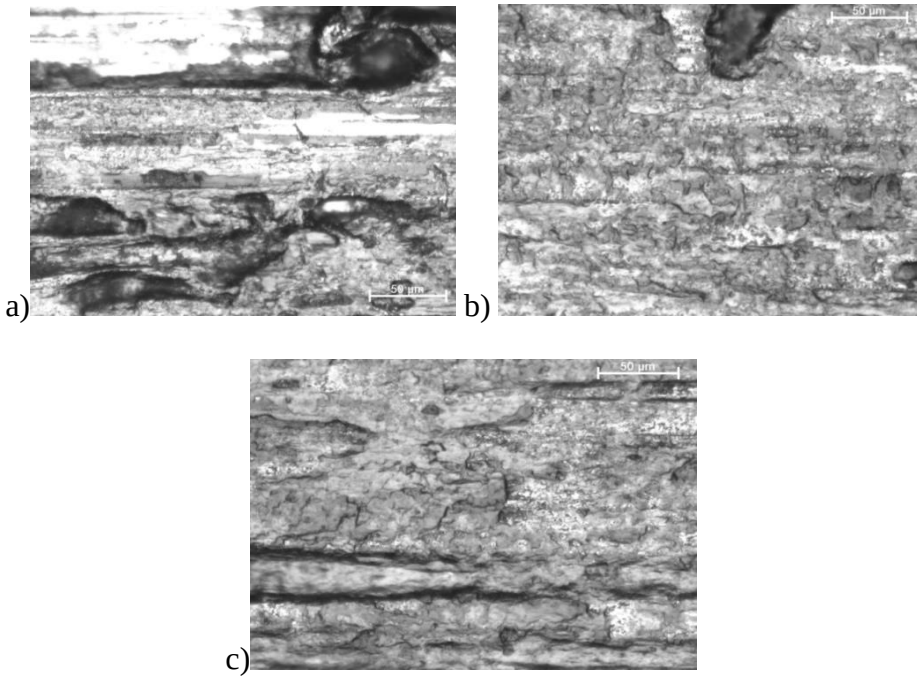

Figure 4.28. Effect on smooth surface-4MPa normal pressure after 3000 cycle

a) Low velocity

b) Medium velocity

c) High velocity

The microscopic images of surface damage for the 4MPa tests for smooth pairs are presented in Figure 4.28. The qualitative images showed less damage than the 2 MPa tests. For the low velocity test, some white spots indicate undamaged portions of the surface. For the high velocity test, there existed some scratches indicating some plowing components during friction. The microscopic image of the undamaged rough specimen, which features coarser grinding than the smooth surface, is shown in Figure 4.29.

The deformed surfaces for rough combination, shown in Figure 4.30, damaged spots were more regular than the smooth case. It indicates less damage occurred for the rough cases for the 2 MPa tests. Moreover, the higher volume of white portions showed proof of undamaged surfaces during friction. There was no distinguishable difference in microscopic images for the three velocity tests.

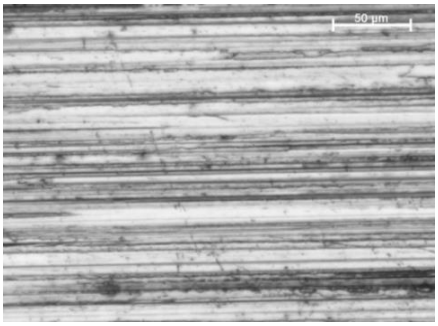

Figure 4.29. Undamaged rough surface

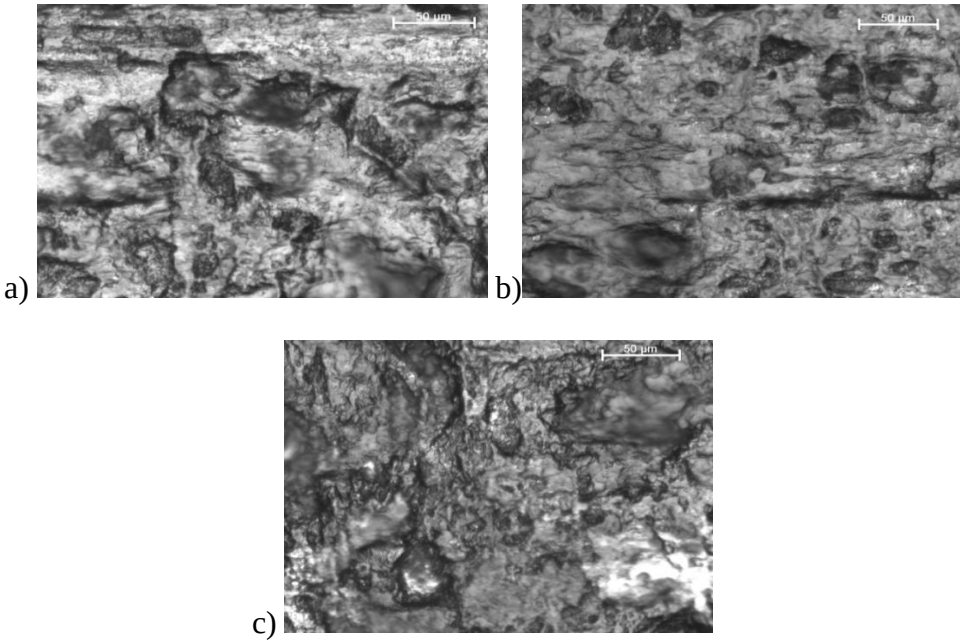

Figure 4.30. Effect on rough surface-2 MPa normal pressure after 3000 cycle

a) Low velocity

b) Medium velocity

c) High velocity

a) 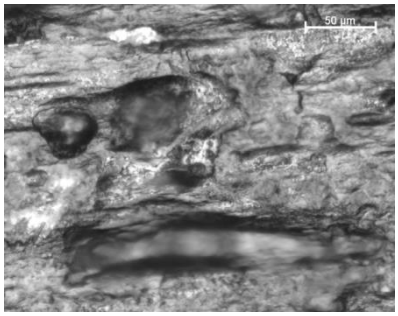 b) 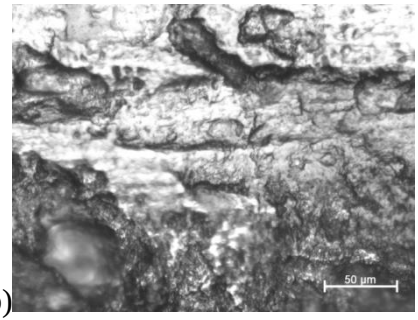

Figure 4.31. Effect on rough surface-4MPa normal pressure after 3000 cycle

a) Low velocity

b) High velocity

Along with the peaks and valleys of damaged surfaces for the 4MPa tests, the low velocity test showed some deep area which clearly indicates adhesive type wear. For the high velocity, the damaged spots were more. The out-of-focus images indicate the three-dimensional profile for the damaged surfaces.

4.7 Variation of Roughness Changes

The variations of surface roughness between the damaged and undamaged surfaces are described in Figure 4.32 for the rough pairs and in Figure 4.33 for the smooth pairs. In these two figures only average roughness values were considered. Here we see less variation of roughness for both the 2 MPa and 4MPa tests, except for the high velocity test. Other roughness parameters measured in this study are listed in charts in Appendix B.

The change of roughness was significant for the smooth-smooth pairs. The most noticeable feature is that, the 2 MPa tests gave more rough surfaces. For the 4MPa tests, smooth surfaces showed less change of roughness.

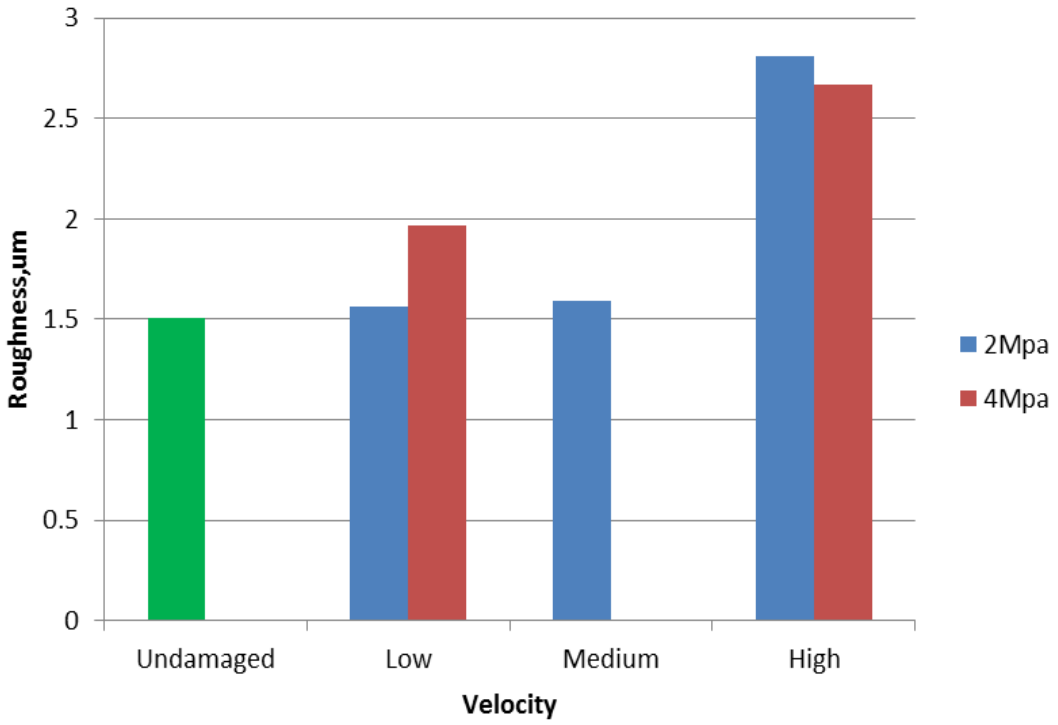

Figure 4.32. Change of roughness by friction for rough-rough pairs

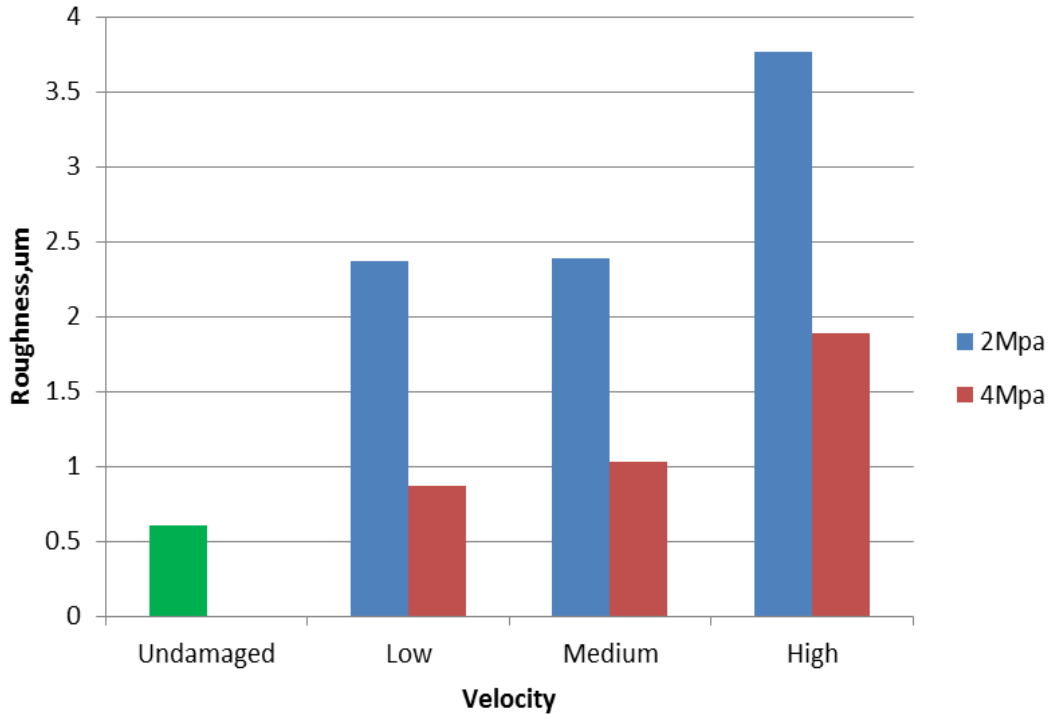

Figure 4.33. Change of roughness by friction for smooth-smooth pairs

4.8 Calculation of Damaged Area

The pattern of surface damage area suggests the contact surface was not the same as the pad dimensions (Figure 4.34). A Matlab™ code was developed to quantify the area of the deformed surface. The code works by counting the pixels of prescribed colors of the damaged surface. The pressure on the deformed surface is termed as deterministic pressure here in Table 4.2.

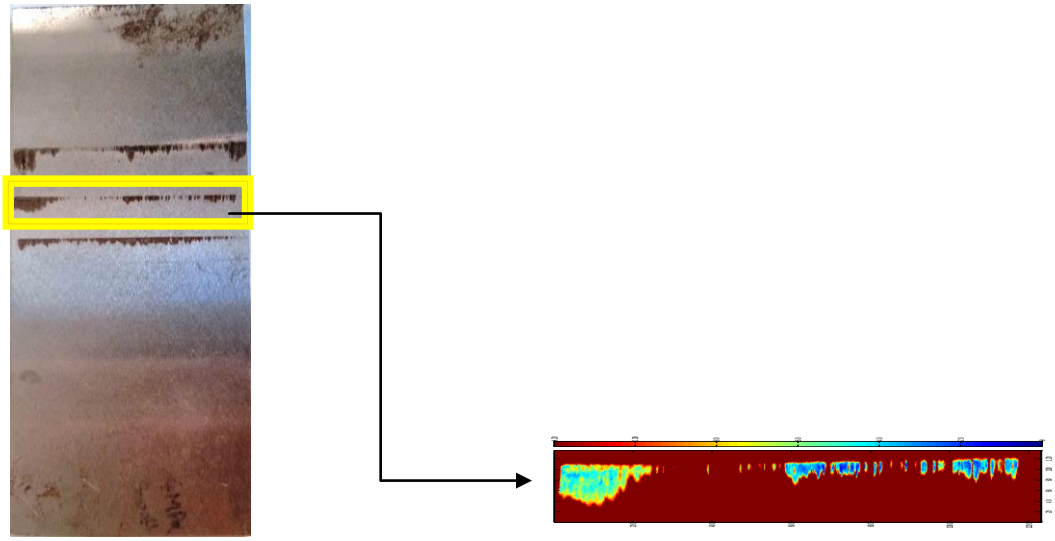

Figure 4.34. Calculation of damaged area (smooth pair medium velocity 4MPa test)

Table 4.2

Chart for Calculating Deterministic Pressures for Different Tests

		2 MPa Test			4MPa Test		
Surface	Velocity	**Area, mm^2**	**Normal Force N**	**Deterministic Pressure, MPa**	**Area, mm^2**	**Normal Force N**	**Deterministic Pressure, MPa**
Rough	**Low**	20.25157	516.1272	**25.48578**	29.4451	1032.254	**35.05691**
	Medium	21.50318	516.1272	**24.00236**	45.10959	1032.254	**22.88326**
	High	18.09674	516.1272	**28.52045**	47.30313	1032.254	**21.82211**
Smooth	**Low**	17.12255	516.1272	**30.14313**	37.29025	1032.254	**27.68162**
	Medium	12.58062	516.1272	**41.02557**	38.06444	1032.254	**27.1186**
	High	27.93543	516.1272	**18.47572**	67.48374	1032.254	**15.29634**

4.9 Analysis of the Results

The mechanics of sliding contacts cannot be defined by a single theory. The repeatability of the events is also low because in each stroke of movement the surface textures are changing. The contradiction with our results and the existing friction theories can be minimized by considering the actual contact (not real contact area of the asperities) of the test pads. For 2MPa and 4MPa tests a perfect flat surface was assumed for the friction pad and bar and uniform pressure distribution along their areas. But the actual contact area was suspected different as damage in bar and pad was only on limited places. It was considered that, the actual contact area was proportional to damaged area, due to plastic deformation during a friction test, and calculated the deterministic pressure.

From figure 4.2 it was observed that there was not any noticeable change in friction energy while changing velocity from low to medium. The general phenomenon (Rabinowicz 1995) used for describing this weak dependence of the sliding velocity is that strength of most solids has small dependence on application rate. For adhesive wear the friction is occurred by plastic failure of micro asperities. If it was assumed that the frictional wear during low and medium velocity was dominated by adhesive wear mechanism then our assumption will coincide to the current experimental data. Actually friction is constant in small range of sliding velocity change, unless the velocity of sliding is too high to be considered as impact for micro asperities. But, there a significant change of AE in high velocity test was found with same travelling distance. High velocity test also encountered high amplitudes (Figure 4.1) and higher number of events. Three possibilities can be suggested for high velocity events,

a) The value of sliding velocity acted as impact
b) The increased area of friction gave a rise of asperity collisions (elastic)

c) There might be a change of wear mechanism (adhesive to abrasive or fatigue)

These possibilities will be cross checked with other results later in this chapter.

From Figure 4.3 to figure 4.6 one can infer that friction related AE is almost independent of surface roughness. While conducting friction tests in a small range of roughness values, it is true for adhesive wear dominated friction. For very smooth surfaces the friction is higher because of the two sliding surfaces are exposed to more small numbers of asperities to each other, hence real contact area is large. On the other hand for rough surfaces the large asperities hinder each other to slide over, and the digging of more material (abrasive wear) can create obstruction of sliding. According to Rabinowicz (1995)for friction in normal engineering practices the intermediate conditions are used, where the two surfaces are relatively smooth and friction is minimum and almost independent of roughness.

Another evident trend for the smooth surfaces is they are giving more AE in low velocity tests and rough surfaces are giving more AE in high velocity tests. The independence of friction, which is frictional energy in this study, on surface roughness does not hold good here. If the deterministic pressures are seen from Table 4.2 it can be realized that all the surface pairs with high deterministic pressure values (Low velocity 4MPa test is only exception) gave more AE events and energy.

The total friction energy should not vary on surface areas or pressure values. But, on a certain threshold and frequency band, many signals with low amplitude signals are disregarded. Hence only high amplitude signals (crossing the threshold) are counted which can be created by localized pressure only. Another possibility that might occur here is that friction mechanisms are changing for high velocity tests. The dependence of surface roughness on frictional AE is not obvious here in this study.

From Figure 4.7 & 4.10 a clear dependence of applied load on frictional AE is seen. Although the number of events is less in 2MPa case, for high velocity smooth test (Figure 4.8) the AE of 2MPa test over passed the 4MPa test AE. The dominance of 2 MPa test AE is due to the different threshold value of these two tests. For 2MPa test the threshold value was 35dB and for 4MPa it was 30 dB. The high HLT time did not let the channels to detect all signals. As, 2MPa test was acquiring only the high amplitude data the total amount of energy for this test became higher. Similar conditions occurred in rough surfaces high velocity case.

The friction signals cannot be considered as they are coming from a single phenomenon. Rather, it may be an outcome from multiple collisions, asperity contact, plastic deformation and reflection of signals that are taking place at the same time. In a single signal, multiple frequencies and features may be observed. The noise to peak ratio for a signal was also higher than a simple lead break test. The comparison study of waveforms in a single test is described in Figure 4.11 to 4.14. Similar frequency spectrum was observed in a test in terms both frequency ranges and frequency components. The dominance of flexural component (A_0 mode) was found throughout the periods of test.

The changing velocity gave an important indication in AE frequency components described in some sample examples in figure 4.15 to 4.17. Though amount of AE events was found independent between low and medium sliding velocity, the higher frequency components were found more in higher velocity tests. This can be explained by (Greenwood-Williamson 1966) & (Alam and Sundaresan 2010). The impulse time taken by the asperities is smaller for higher velocities. So, high frequencies are more likely to be present in this case.

The comparison study of waveforms (Figure 4.18 to 4.21) in varying roughness gave clear pattern of frequency ranges and frequency components. This can be easily explained by

asperity collisions (both elastic and plastic) and breakage of adhesive junctions. Smooth surfaces have smaller asperities that make less time of contact between them. This creates high frequency in smooth surface sliding contact.

The effect of normal pressure on frequency components is evident in Figure 4.22 to 4.25. As normal pressure is decreased there will be more chance of collisions of the peaks with less time duration. It will increase the chance of higher frequency. Between the 2MPa test (figure 4.22) and the 4MPa test (figure 4.23 a), the 2MPa had a lower deterministic pressure (Table 4.2) and it is giving more high frequency component. Similarly, Figure 4.25 manifests more high frequency component for 4MPa test as it had lower deterministic pressure.

Figure 4.24 to Figure 4.29 describes the topography seen in an optical microscope. All of the images are giving similar pattern of damage. The surface profiles were irregular in pattern which signifies adhesive type of wear. There existed some scratches in few high velocity test surfaces which are a possible evidence of abrasive wear. The black spots found on the surfaces were result of corrosion. It might not be impossible that there was some corrosive wear.

The pressure values found in Table 4.2 and the changed roughness values have very good agreement. For smooth case all the 2MPa tests had higher roughness values, in damaged surface, than the 4MPa tests. The 4MPa rough surface low velocity test also had higher deterministic pressure, provided higher roughness than corresponding 2MPa (Figure 4.32). It is logical in this sense that more localized pressure should create deeper effect (like scratch) on surface and hence roughness.

CHAPTER 5

Discussion and Future Research

To establish effective methodology of structural health monitoring for sliding contact, the primary requirement is to determine the nature of AE for friction. For understanding the nature of AE the best way is to determine its trend by changing its parameters. In this study three parameters were considered to characterize frictional AE.

The tribological study involved in it comprises several issues like elastic contact, plastic contact, asperity distribution, real contact of the surfaces, wear mechanisms etc. The detailed study of these issues and their possible effect on AE signals and waveforms are beyond the scope of current research. The friction surface where there is no wear is dominated by elastic collisions of the asperities. The plastic deformation of asperities is a possible outcome. After that when wear initiates, like the present test conditions, it starts with adhesive wear mechanism. After certain cycles (depends on the conditions) it may lead to the abrasive wear which is catastrophic for structure.

From the microscopic images it was evident that adhesive wear was occurred. Some wear in friction pad surface was also observed which was made of a slightly harder material. (Bhushan 1990) suggested material transferred by adhesion to harder surface is detached by fatigue process.

In all the previous researchers who conducted studies with high threshold values endeavored to correlate the AE with wear. In the current research, the threshold value as low as 30 dB was successfully utilized. It allowed exploring more data region in this research. It helps to provide indication of friction well ahead. The exact transition from elastic collisions to plastic wear is still unknown in terms of AE.

Parameters other than sliding velocity, normal pressure and surface roughness were not controlled in this study. All tests were carried out in room temperature and humidity. Insulation was used in the mounting positions of the steel bar to provide isolation from hydraulic noise and electrical signals.

From the current study the following can be concluded

- High velocity gives higher range of amplitude and AE energy in friction
- High velocity gives high frequency components in waveforms
- Effect of surface roughness on frictional AE can be established by maintaining same pressure distribution of the surface
- Smooth surface give rise of high frequency component in waveform compared to rough surfaces.
- Higher normal load gives rise of AE
- Higher normal pressure decreases the possibility of high frequency components in the waveforms.

For future research more control over surface contact area is important to establish direct relationship with surface roughness and AE energy. Proper alignment of the fixture and redesign of the friction pad can contribute more consistent results. The Hit Lockout Time parameter which was set 1000 micro second in this study found long as many data missed in this time. All the signal acquisition parameters should be reconsidered. More roughness and velocity combination studies can establish the actual mechanisms for waveform pattern and underlying physics.

References

Alam, T. and M. J. Sundaresan (2010). "CHARACTERIZATION OF FRETTING RELATED AE SIGNALS." MS Thesis, Department of Mechanical Engineering, North Carolina A&T State University.

Archard, J. F. and W. Hirst (1956). "The wear of Metals under unlubricated conditions." http://www.jstor.org.

Asamene, K. and M. Sundaresan (2012). "Analysis of experimentally generated friction related AE signals." Wear **296**(1-2): 607-618.

ASTM Standard G40, 2013, "Standard Terminology Relating to Wear and Erosion" ASTM International, West Conshohocken, PA, 2013, DOI: 10.1520/G0040-13, www.astm.org.

Baranov, V. M., et al. (1997). "Modelling of the parameters of AE under sliding friction of solids." Wear **202**(2): 125-133.

Benabdallah, H. S. and D. A. Aguilar (2008). "AE and Its Relationship with Friction and Wear for Sliding Contact." Tribology Transactions **51**(6): 738-747.

Bhushan, B. (1990). Tribology and mechanics of magnetic storage devices, Springer-Verlag.

Diamanti, K. and C. Soutis (2010). "Structural health monitoring techniques for aircraft composite structures." Progress in Aerospace Sciences **46**(8): 342-352.

Fan, Y., et al. (2010). "Modelling acoustic emissions generated by sliding friction." Wear **268**(5-6): 811-815.

Ferrer, C., et al. (2010). "Discrete AE waves during stick–slip friction between steel samples." Tribology International **43**(1-2): 1-6.

Greenwood, J., and Williamson, J., 1966, "Contact of Nominally Flat Surfaces," Proc. Royal Society of London. Series A, Mathematical and Physical Sciences, 295, pp. 300-319.

Hase, A., et al. (2009). "AE in Elementary Processes of Friction and Wear: In-Situ Observation of Friction Surface and AE Signals." Journal of Advanced Mechanical Design, Systems, and Manufacturing **3**(4): 333-344.

Hase, A., et al. (2012). "Correlation between features of AE signals and mechanical wear mechanisms." Wear **292-293**: 144-150.

Hase, A., et al. (2008). "The relationship between acoustic emissions and wear particles for repeated dry rubbing." Wear **265**(5-6): 831-839.

Ito, S., et al. (2009). "The relationship between AE and dissipation energy for fretting wear." Tribology International **42**(2): 236-242.

James Li, C. and S. Y. Li (1995). "AE analysis for bearing condition monitoring." Wear **185**(1–2): 67-74.

Kilundu, B., et al. (2011). "Cyclostationarity of Acoustic Emissions (AE) for monitoring bearing defects." Mechanical Systems and Signal Processing **25**(6): 2061-2072.

Mason, W. P. (2012). Physical Acoustics V11: Principles and Methods, Elsevier Science.

Mba, D. and J. Z. Sikorska (2008). "Challenges and obstacles in the application of AE to process machinery." Proceedings of the Institution of Mechanical Engineers, Part E: Journal of Process Mechanical Engineering **222**(1): 1-19.

Menezes, P. L., et al. (2006). "Effect of Roughness Parameter and Grinding Angle on Coefficient of Friction When Sliding of Al–Mg Alloy Over EN8 Steel." Journal of Tribology **128**(4): 697.

Menezes, P. L., et al. (2008). "On the effect of surface texture on friction and transfer layer formation—A study using Al and steel pair." Wear **265**(11-12): 1655-1669.

Miller, R. K., et al. (2005). AE Testing, American Society for Nondestructive Testing.

Rabinowicz, E. (1995). Friction and Wear of Materials, Wiley.

Rose, J. L. (2004). Ultrasonic Waves in Solid Media, Cambridge University Press.

Sun, J., et al. (2005). "Wear monitoring of bearing steel using electrostatic and AE techniques." Wear **259**(7-12): 1482-1489.

Unnþórsson, Rúnar (2013). Hit Detection and Determination in AE Bursts, AE - Research and Applications, Dr. Wojciech Sikorski (Ed.), ISBN: 978-953-51-1015-6, InTech, DOI: 10.5772/54754.

Vahaviolos, S. J. (1999). Acoustic Emission: Standards and Technology Update, ASTM.

Whitehouse, D. J. (2004). Surfaces and their Measurement, Elsevier Science.

Appendix A

1. Calculation of Equivalent Voltage of Load cell corresponding to 2 MPa pressure

Area of the Friction zone =50.8X5.08 mm^2

= 258.064 mm^2

Force =Pressure X Area

=2X258.064

= 516.128 N

=52.612 Kg force

Load (kg) = $(1.2468X10^2)$ X Voltage - 6.2497X10

[Formula given by load cell manual]

So, Voltage = (52.612 +62.497)/ $(1.2468X10^2)$

=0.9 Volt

2. Source Location Calculation

For rough 4MPa test

Considering AE velocity in the plate 5 mm/μ sec

Maximum Distance of friction area from Channel1=57 mm

Maximum Distance of friction area from Channel1=92 mm

So, any signal coming from friction area should reach both channels within time

= (92-57)/5 μ s

= 7 μ s

Appendix B

Roughness Calculation Chart

For Smooth Surface,

	Ra, μm	**Rq,** μm	**Rz,** μm	**Rt,** μm
Undamaged Surface	**0.6**	**0.81**	**8.44**	**10.27**
Smooth 2 MPa				
Low1	1.88	2.51	22.36	25.75
Low2	1.45	2.02	21.55	24.72
Low3	3.78	5.19	36.27	37.69
Average	**2.37**	**3.24**	**26.7267**	**29.3867**
Medium1	3	4	30.14	32.11
Medium2	2.42	3.46	26.55	28.27
Medium3	1.74	2.77	32.59	34.66
Average	**2.38667**	**3.41**	**29.76**	**31.68**
High1	1.12	1.63	14.69	16.17
High2	3.25	4.35	3.47	33.68
High3	6.93	9.05	43.61	45.39
Average	**3.76667**	**5.01**	**20.59**	**31.7467**
Smooth 4MPa				
Low1	0.94334	1.49	13.29	14.91
Low2	0.68321	0.98462	11.15	14.11
Low3	0.98326	1.42	12.86	13.45
Average	**0.86994**	**1.29821**	**12.4333**	**14.1567**
Medium1	1.31	1.78	15	16.85
Medium2	0.9613	1.51	14.31	14.73
Medium3	0.80722	1.26	12.87	14.32
Average	**1.02617**	**1.51667**	**14.06**	**15.3**
High1	1.92	2.49	14.48	14.74
High2	1.87	2.45	13.19	13.32
High3	1.86	2.42	15.69	16.24
Average	**1.88333**	**2.45333**	**14.4533**	**14.7667**

Roughness Calculation Chart (Continued)

For Rough Surface,

	Ra, μm	**Rq,** μm	**Rz,** μm	**Rt,** μm
Undamaged Surface	**1.51**	**0.81**	**8.44**	**10.27**
Rough 2 MPa				
Low1	1.85	2.4	13.93	14.19
Low2	1.28	1.83	13.24	14.24
Low3				
Average	**1.565**	**2.115**	**13.585**	**14.215**
Medium1	1.7	2.3	16.76	17.6
Medium2	1.91	1.51	15.28	17.06
Medium3	1.16	1.74	18.47	19.38
Average	**1.59**	**1.85**	**16.8367**	**18.0133**
High1	2.24	2.98	19.63	20.21
High2	3.38	4.19	24.41	25.81
Average	**2.81**	**3.585**	**22.02**	**23.01**
Rough 4MPa				
Low1	1.97	2.8	20.59	22.44
Low2	1.86	2.82	20.94	22.61
Low3	2.07	2.8	20.49	21.38
Average	**1.96667**	**2.80667**	**20.6733**	**22.1433**
High1	2.39	3.3	21.9	23.62
High2	1.52	2.39	18.3	19.33
High3	4.1	4.93	26.1	28.87
Average	**2.67**	**3.54**	**22.1**	**23.94**